Chapter 3 Surface Optimization of Gold Nanoparticles for Controlled Delivery into Cancer Cell Nuclei

Some of the material in this chapter has been adapted with minor modifications from the following article which has been submitted for publication:

Curry, T., Qian, W., Che, Y., & Kopelman, R. Surface Optimization of Gold Nanoparticles for Controlled Delivery into Cancer Cell Nuclei. *Submitted*.

3.1 Introduction

The interest in delivering nanoparticles into cell nuclei mainly stems from considerations of imaging and therapy.[1-3] Gold nanoparticles have many appealing imaging properties, including the ability to generate extraordinary enhancement of Raman scattering from adsorbed molecules, size- and shape-dependent intensification of optical absorption, and tunable scattering throughout the visible and near infrared (NIR) region.[4] The aforementioned properties, coupled with their small size, chemical inertness and biocompatibility (non-toxicity), have led to gold nanoparticles being used widely, not only for cellular imaging and biomedical diagnostics but also for drug and gene delivery, and for photothermal therapy.[1-3,5-10] For almost all these biomedical applications, intracellular delivery of gold nanoparticles (NPs) is required and there have been a number of studies investigating how size, shape, and surface charges of gold

NPs affect their uptake and intracellular fate[3, 11-13]. Although it is not very difficult to achieve intracellular delivery of gold NPs, *selectively* delivering them to the proper subcellular compartment still remains a significant practical challenge. Recently, the development of technologies that facilitate targeted delivery of gold NPs to specific subcellular organelles has been generating widespread interest, since successful use of gold NPs in biology and medicine heavily relies on selectivity and on efficiently delivering them to a particular organelle, in order to exert the therapeutic and/or diagnostic function on the organelle.

Among the large variety of subcellular organelles, such as the nucleus, mitochondria, Golgi apparatus, and endoplasmic reticulum, the nucleus is a major target for macromolecules and nanoparticles with potential diagnostic and therapeutic applications, because the genetic information of the cell and its transcription machinery reside there. Novel diagnostic and therapeutic strategies (for example, gene therapy), enabled by safe and efficient delivery of drug molecules and nanoparticles into the nucleus, are heralded by many as the ultimate treatment for severe and intractable diseases, including cancer, viral infections, and inherited genetic disorders. However, most nanomaterials and macromolecules are incapable of reaching the cell nucleus on their own, because of the need of overcoming an array of biological barriers carefully honed by evolution; for example, the cellular membrane and the nuclear envelope. An elegant method for targeted delivery of NPs involves modifying their surface with peptides [14-18] Tkachenko et al. conjugated synthetic nuclear localization signal (NLS) peptides to gold NPs using bovine serum albumin (BSA) as carrier

proteins and demonstrated nuclear delivery of NPs by using video-enhanced color differential interference contrast microscopy[19]. Another approach aimed at enhanced nuclear delivery of Au NPs was presented by Brust et al. in which PEG-stabilized Au NPs were modified with a combination of NLS and cell penetration peptides (CPPs), for example, the oligopeptides TAT (AGRKKRRWRRR) from HIV and Pntn (GRQIKIWFQNRRMKWKK) from Antennapedia protein from Drosophila, each appended to CALNN[20]. They observed that a combined strategy using NLS peptide and CPPs peptide leads to synergistic effects on penetrating barriers of cellular membrane and the nuclear envelope.

Although several studies demonstrating nuclear delivery of gold NPs have been reported, there is still a need for a study that thoroughly investigates how the surface chemistry of gold NPs affects the complex processes that govern transport into the cell nucleus and how to optimize the proportion of functional ligands conjugated onto the surface of gold NPs for efficient nuclear delivery. In the present study, chemically controlled surface engineering of gold nanoparticles enable controlled nuclear delivery. Two types of peptides, cysteine $(RGD)_4$ (RGDRGDRGDRGDPGC) and NLS (CGGFSTSLRARKA), are conjugated to partially PEGylated Au NPs. $(RGD)_4$ peptides are used here for targeting integrin- a cancer marker that is overexpressed on the cytoplasm membrane of most types of cancer cells, enabling the transport of gold NPs into the cells via receptor mediated endocytosis. NLS peptides derived from SV-40 large T antigen are used for targeting the cell nucleus via recognizing and

binding to nuclear transport receptors, especially importin-β/karyopherin-β class receptors, which subsequently ferry the gold NPs into cell nuclei through nuclear pore complexes (NPCs). The initial uptake and subsequent nuclear delivery pathway of the nanoparticles in the HeLa cells is pictured in Figure 3.1. The gold NPs used in our experiments were fabricated by a physical method, using femtosecond laser ablation of a gold target in ultrapure water. In contrast to gold NPs fabricated by chemical methods, this preparation method provides a chemical free, *virgin* gold surface. As clarified in our previous study [21], such extra-pure *virgin* surfaces allow highly efficient and controllable surface functionalization of gold nanoparticles, compared to gold NPs produced by wet chemical methods. The use of gold nanoparticles with *virgin* surfaces enabled the undertaking of a systematic study on how nanoparticle-cell interactions are dictated by the surface chemistry of the NPs and the ability of optimizing the ratio of functional ligands so as to achieve optimal nuclear delivery.

3.2 Background

Generation of nanoparticles via pulsed laser ablation was first described by Hengleing and Fotjtik [22,23] (in either an organic solvent, aqueous solution, or plasma) and by Neddersen *et al.* [24] in 1993. The invention of the femtosecond laser has increased the interest in this method of metallic nanoparticle production as it eliminates many of the drawbacks associated with the use of nanosecond lasers[25]. One major advantage of producing gold nanoparticles via pulsed laser ablation in ultrapure water is the resulting, completely “virgin” nanoparticle

surface, devoid of any surfactants, salts, or other stabilization agents, unlike chemically produced nanoparticles. A recent study conducted by Qian, *et al* [21] detailed the production and controllable pegylation of gold nanoparticles that were produced through femtosecond laser ablation of a 99.99% pure gold target in ultrapure water. In the study, the nanoparticles were systematically characterized and compared to commercially available, chemically produced gold nanoparticles of the same size. Both types of gold nanoparticles were covered with varying amounts of PEG 20K via thiol bonding and the laser generated nanoparticles exhibited surprising better colloidal stability compared to the purchased nanoparticles. Further, the exact amount of PEG 20K needed to provide a complete monolayer was determined and this finding demonstrates the ability to very precisely control the surface chemistry of the laser-generated nanoparticles. This is not the case for the commercially bought, citrated capped nanoparticles; many studies have found that attaching various moieties to chemically produced gold nanoparticles is mediated through ligand exchange and a dynamic equilibrium which in turn requires that an excess of the moieties be kept in solution in order to maintain colloidal stability. [26,27] Drawing on the success of this previous study, the gold nanoparticles utilized in the experiments described in this chapter were also produced via femtosecond laser ablation and strategically surface engineered toward the goal of efficient nuclear delivery to cancer cells.

3.3 Materials & Methods

3.3.1 Materials

Dulbecco's Modified Eagle medium (DMEM 1195 & 21063), Dulbecco's Phosphate Buffered Saline (DPBS), fetal bovine serum (FBS), penicillin-streptomycin glutamine, and the Live/Dead *Bac*light Bacterial Viability Kit were all purchased from Invitrogen. 100mm and 35mm Petri dishes were purchased from BD Biosciences. 8 well chambered plates were purchased from Fisher Scientific. Thiolated poly(ethlylene glycol) with a molecular weight of 5 kiloDaltons was purchased from Nancos (New York, NY). Rectangular gold target (16mm long, 8mm wide, 0.5mm thick) was purchased from Alfa Aesar. $(RGD)_4$ and NLS peptides were purchased from RS Synthesis (Louisville, KY). The water used throughout the experiment was de-ionized (DI) water, purified by a Milli-Q system from Millipore Co.

3.3.2 Cell Culture

HeLa 229 cells (American Type Culture Collection) were grown in Dulbecco's modified Eagle medium (DMEM 11995) supplemented with 10% FBS and 1% penicillin-streptomycin at 37°C with a 5% CO_2 atmosphere in a humidified incubator. Cells were plated and grown in 100mm and in 35mm Petri dishes.

Cell imaging:

All live cell imaging was completed using an Olympus IX71 inverted microscope (Olympus America Inc., Melville, NY), using the bright field and both a 20X and a 40X objective. Transmission Electron Microscopy of fixed and

sectioned cells was completed using a Phillips CM100 electron microscope at 60kV. Images were recorded digitally, using a Hamamatsu ORCA-HR digital camera system operated using AMT software (Advanced Microscopy Techniques Corp., Danvers, MA).

3.3.3 Nanoparticle Fabrication

Chemical free, gold nanoparticles with virgin surfaces were synthesized using a previously established femtosecond laser ablation method with the following laser parameters.[21] Femtosecond pulses delivered from commercial available Ytterbium-doped femtosecond fiber laser (FCPA μJewel D-1000, IMRA America) at a repetition rate of 100 kHz with 10 μJ pulse energy and 700 femtosecond pulse width centered at wavelength of 1.045 μm were focused onto a spot size of about 50 μm on gold metal plate (99.99% purity), which was placed on the bottom of a glass vessel filled with 20 ml deionized water (18 MΩ cm). A representative extinction spectrum and a representative transmission electron microscopy (TEM) image of laser generated gold nanoparticles are shown in Figure 3.2. The extinction spectrum was characterized by the presence of a peak around 520 nm, arising due to localized surface plasmon resonance (LSPR), and the spectral feature below 450 nm reflects gold intraband transitions, since this sample was prepared in deionized water without involving any chemical components except the gold target itself. The average diameter of gold nanoparticles was determined to be 20 nm by evaluating more than 500 nanoparticles.

3.3.4 Nanoparticle Surface Modification

The amount of thiol-terminated poly(ethylene glycol) with a molecular weight of 5000 required to form a complete monolayer on the surface of the gold nanoparticles was first experimentally determined. Varying molar ratios, between 10 to 3000 per nanoparticle, of PEG 5K was added to the nanoparticle solution and allowed to stir for 3 hours. The resulting size of the nanoparticles was then measured using Dynamic Light Scattering DLS on a Nano-ZS90 Zatasizer (Malvern Instruments, Westborough, MA). The size of the nanoparticle increased with the increasing molar ratio of PEG 5K until approximately 400, after which the size of the nanoparticle remains constant, shown in Figure 3.3. This experimental finding provides evidence that the maximum molar ratio of PEG 5K required to form a complete monolayer is approximately is 400:1.

Subsequent surface modifications to facilitate efficient nuclear delivery were completed by a series of chemical reactions, via “Sequential Conjugation” as outlined here: Thiolated PEG 5K was attached directly to the nanoparticle surface (bond strength 197.4 kJ/mol)[28], so as to increase colloidal stability.[21] Next, $(RGD)_4$ peptide was attached directly to the nanoparticle surface, to facilitate cellular uptake. Lastly, a nuclear localization sequence peptide (NLS) was attached directly to the nanoparticle surface to enable nuclear delivery. All peptides were conjugated to the gold nanoparticle surface via thiol bonding. The surface modifications were completed in DI water and after adding each moiety, the solution was allowed to stir with the nanoparticles at room temperature for 3

hours to ensure complete conjugation. Finally, the modified gold nanoparticles are allowed to stir overnight. The solution was then washed via centrifugation at 15,000g for 30 minutes to remove any unattached molecules. The modified gold nanoparticles were redispersed in PBS buffer with a pH of 7.4.

3.3.5 Concentration Study

Gold nanoparticles prepared with molar ratios of 150 PEG 5k and 1000 $(RGD)_4$ peptide per gold nanoparticle were added to cells to achieve varying overall nanoparticle concentrations between 1 nM and 100 pM and allowed to incubate with the cells for 24 hours. After incubation, the nanoparticles still in solution and cell media were removed. The cells were then washed twice with DPBS to remove any free gold nanoparticles. New clear media was immediately added to the cells and each dish was imaged.

3.3.6 Optimization of Surface Modifications

3.3.6a PEG 5K Optimization

An excess amount of PEG 5K (based on 1000 PEG 5k per NP) was added to the gold nanoparticles and allowed to stir for three hours, after which the unattached PEG was washed out of the solution. Gold nanoparticles were also prepared with PEG 5K (attached to the surfaces) with molar ratios ranging between 150 and 1000 per nanoparticle; $(RGD)_4$ peptide was subsequently added in an excess amount to fill any empty space on the nanoparticle surface and facilitate cellular uptake. After the surface modifications were complete, all

of the nanoparticles were washed and resuspended in PBS. The nanoparticle solution was then diluted with culture media so as to achieve final gold nanoparticle concentrations of 100 pM, and then added to cells. The cells were allowed to incubate with the gold nanoparticles for 24 hours, after which the solution was aspirated and the cells were washed with DPBS, three times, to remove any free gold nanoparticles. New clear media was added to the cells and each concentration was imaged on the microscope.

3.3.6b $(RGD)_4$ Optimization

Gold nanoparticles were prepared with molar ratios of 200 PEG 5k, and with $(RGD)_4$ peptide in varying molar ratios, between 200 and 500 per nanoparticle. The cells were allowed to incubate with the gold nanoparticles for 24 hours, after which the solution was aspirated and the cells were washed with DPBS three times to remove any free gold nanoparticles. New clear media was added to the cells and each concentration was imaged.

3.3.6c Incubation time

Gold nanoparticles that had been modified with PEG 5K, $(RGD)_4$, and NLS 200/400/800 per gold nanoparticle, respectively, were added to cell media so as to achieve a concentration 100 pM. The nanoparticles were allowed to incubate with cells for up to 48 hours. At several intermittent time points the gold nanoparticle solution was aspirated and the cells were washed with DPBS three

times to remove free nanoparticles. New clear media was added to the cells and bright field images were then taken of each sample.

3.3.6d Verification of nuclear delivery

Various samples that were initially imaged, using bright field, were then fixed in 2.5 percent glutaraldehyde, in 0.1 M Sorensen's buffer, pH 7.4, overnight, at 4°C. After several buffer rinses, the cells were postfixed using 1% osmium tetroxide in buffer. The cells were then rinsed in doubly distilled water to remove phosphate salt and then en bloc stained with aqueous 3% uranyl acetate for one hour. The samples were dehydrated in ascending concentrations of ethanol, rinsed two times in 100% ethanol and embedded with epoxy resin. The samples were then ultra-thin sectioned into 70 nm slices and stained with uranyl acetate and lead citrate. These sections were then fixed onto TEM grids and imaged to test for the presence of the gold nanoparticles inside of the nucleus.

3.4 Results and Discussion

3.4.1 Concentration Study

The first goal *before* attempting nuclear delivery was to achieve the most efficient cellular uptake, i.e. low gold nanoparticle concentration in solution coupled with high cellular uptake. Toward this end, the virgin nanoparticle surface was only modified to ensure colloidal stability (PEG 5K) and facilitate cellular uptake ($(RGD)_4$), no NLS was attached to the nanoparticle surfaces in this study. After 24 hours of incubation, very few gold nanoparticles were

observed inside the cells that had been exposed to the lower concentrations of 10 and 32 pM. In contrast, numerous gold nanoparticles had been taken up by cells that had been incubated with 100 pM or 1 nM, with the majority of the nanoparticles surrounding the nucleus of the cells (Figure 3.4). Gold nanoparticles, both with and without surface modifications, are currently being utilized by many groups in a variety of different types of research studies; however, the lower limits of the concentrations used in these studies are typically in the nanomolar range,[11,13, 29,30] with few groups utilizing lower concentrations. Our findings demonstrate that highly efficient intracellular delivery is achieved with a concentration that is *at least* an order of magnitude less than what has been previously reported. All subsequent experiments were conducted with gold NP concentrations of 100 pM.

3.4.2 PEG 5K Optimization

The role of PEG 5k is to enhance the solubility and colloidal stability of the nanoparticles by providing a steric barrier on the surface of the nanoparticle. For the purposes of this study, colloidal stabilization combined with having a large fraction of the nanoparticle surface remaining available for the attachment of other targeting moieties was necessary. Thus, optimization of the PEGylation of the nanoparticle must yield both *stable* and *targetable* nanoparticles, i.e. sufficient but not too much PEG surface coverage. To investigate how best to accomplish this, gold nanoparticles were modified with either PEG 5K only, or with both PEG 5K and $(RGD)_4$ in varying ratios, shown in Figure 3.5A. After 24

hours incubation, the gold nanoparticles with *only* PEG 5K attached to the surface did not enter the cells. However, with the addition of $(RGD)_4$ peptide to the surface of the gold nanoparticles, along with the PEG 5K, the cellular uptake increased as the molar ratio of PEG 5K increased, up to 200 per nanoparticle. However, the uptake decreased after the ratio was increased to 300-500 PEG 5K per nanoparticle. This result indicates that the conjugation of molar ratios of more 300 PEG 5K to the nanoparticles does not leave enough surface area for the attachment of $(RGD)_4$, resulting in much lower binding affinities and, consequently, less uptake into the cancer cells. These findings are summarized in Figure 3.4. The molar ratio of 200 PEG 5K per nanoparticle was found to be the optimal condition for achieving both stability and efficient cellular uptake, and was thus used in subsequent studies. We also note that the addition of PEG to the nanoparticle surfaces also adds an additional biocompatibility characteristic that will be crucial in future *in vivo* studies [31-33].

3.4.3 $(RGD)_4$ Optimization

The aims of the $(RGD)_4$ optimization were to establish the minimum amount of $(RGD)_4$ required for cellular uptake and thereby to maximize the available surface area left for attaching NLS, for achieving nuclear delivery. Our studies revealed that the combination of the molar ratios of 200 PEG 5K and 200 $(RGD)_4$ per nanoparticle was ineffective in achieving cellular uptake into the cancer cells; however, increasing the molar ratio of the $(RGD)_4$ per nanoparticle beyond this lower limit improved the cellular uptake noticeably. The minimum

amount of $(RGD)_4$ required to facilitate cellular uptake was found to be 300 $(RGD)_4$ per nanoparticle, coupled with 24 hours incubation time (Figure 3.5B). To ensure that adequate amounts of NPs were taken up by the cells, a molar ratio of 400 $(RGD)_4$ was thus used in the subsequent studies, along with a molar ratio of 800 NLS per nanoparticle. A control experiment was completed in which cells were incubated for 24 hours with gold NPs that had the molar ratios of 200 PEG 5K and 500 NLS molecules attached per nanoparticle. Only a small amount of the nanoparticles were taken up by the cells in the absence of $(RGD)_4$ on the nanoparticle surface. Taken together, the addition of the three different moieties to the nanoparticle surface provides a synergistic effect resulting in the optimal uptake of the NPs by the cancer cells.

3.4.4 Incubation time

Cancer cells were first checked 12 hours following the addition of the gold nanoparticles; however, very few nanoparticles could be seen inside the cells (*Data not shown*.). After 24 hours incubation time, many gold nanoparticles were internalized within the cells. Furthermore, in the cases of more extensive incubation times, up to 48 hours, the majority of the gold nanoparticles that were taken up into the cells had accumulated predominantly around and within the nucleus of the cells, causing the nucleus to appear very dark (Figure 3.5C). It should be noted that in this case of an extended incubation time, the cells continue to divid and the daughter cells also have gold nanoparticles internalized within them. Many studies involving nuclear-targeted gold nanoparticles utilize

incubation time periods between a few hours and 24 hours; however, in studies employing shorter incubation time periods, most nanoparticles were found to be very near the nuclear envelope, i.e. nuclear delivery was achieved with low efficiency.[13] Furthermore, in a study where targeted gold nanoparticles were injected directly into cells very near the nucleus, nuclear uptake was still not achieved very efficiently over short time periods.[12] Although the cells utilized in our experiments divide approximately every 24 hours, efficient intracellular delivery is achieved within the parent cells during the first 24 hours, such that efficient nuclear delivery is possible and was observed in the daughter cells.

3.4.5 Confirmation of Nuclear Delivery

Positive confirmation of nuclear delivery was obtained by observing the presence of the gold nanoparticles in the nucleus of cells that were *healthy* at the time of fixation, as evidenced by undisrupted cellular membranes. Figure 3.6 is a representative TEM image affirming the presence of gold nanoparticles within the nucleus of the cell, with the corresponding bright field image of the same sample before fixation. Gold nanoparticles were found predominantly in the nuclei of the cells, however, some nanoparticles were also found encased in the lysosome/endosome complex, as well as in the cytosol, demonstrating the different stages involved between the times of cellular uptake and nuclear delivery.

3.5 Conclusions

As noted in previous works,[19,34] multiple peptides are required to facilitate effective and efficient nuclear delivery, which entails entering the cells, escaping or avoiding the endosome/lysosome complex, and passing through the nuclear envelope. Many studies have demonstrated that no single functional modification of the gold nanoparticle surface has the ability to achieve all of the required steps, and in the case of multifunctional modification, optimization is at best specific to the cell line under observation. In the present study, optimized nuclear delivery of gold nanoparticles into immortalized HeLa cells was achieved by modifying the surface of gold nanoparticles having “virgin surfaces” with multiple peptides, in addition to PEGylation. Each step of the “Sequential Conjugation” method used in modifying the gold nanoparticles was optimized to achieve the most effective intracellular uptake and was confirmed via light microscopy. The final step of efficient nuclear delivery was confirmed using both light and Transmission Electron Microscopy.

Due to the global applicability of the methods utilized in the present study and the unique “virgin-surfaced” nanoparticles, similar optimization for nuclear delivery may be readily achieved for other cell lines, by using the described approach and the appropriate targeting moieties. We note that the absence of any chemical residues on the surface of the nanoparticles is of dire importance as it enabled:

1. Attachment of *known* amounts of targeting molecules to the nanoparticle surfaces,

2. High cellular uptake with no resulting toxicity, and
3. Extended incubation times with no resulting toxicity.

The methods and findings of this study are expected to contribute to the advancement of nanoparticle facilitated nuclear diagnostics and therapeutics, by providing a method through which the NPs assuredly reach the interior of the nucleus rather than being trapped outside it in an endosome/lysosome complex or within the nuclear envelope.

3.6 Acknowledgements

The authors would like to acknowledge Sasha Meshinchi, Chris Edwards and the rest of the staff of Microscopy and Imaging Analysis Laboratory at the University of Michigan-Ann Arbor.

3.7 Figures

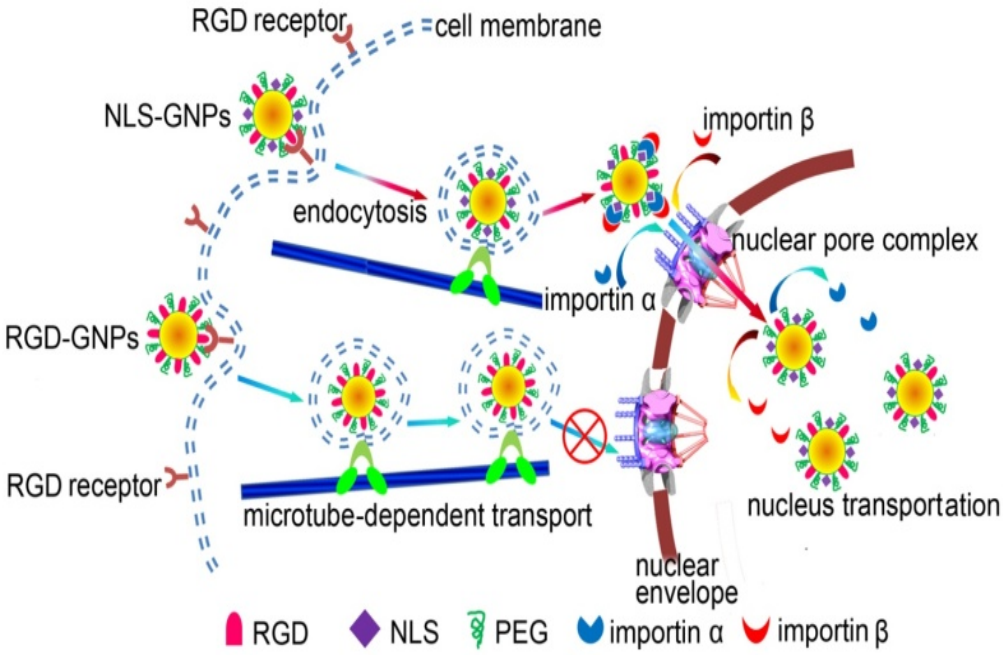

Figure 3.1: Schematic diagram of targeted delivery of multi-targeted, biocompatible Au NPs into cell nucleus. The function of PEG is to maintain stability of Au NPs in media and prohibit non-specific binding to cells. RGD enables binding of the Au NPs to receptors on the cell membrane and induces intracellular delivery via endocytosis. NLS enables binding of the Au NPs to importin, which mediates nuclear transport.

A

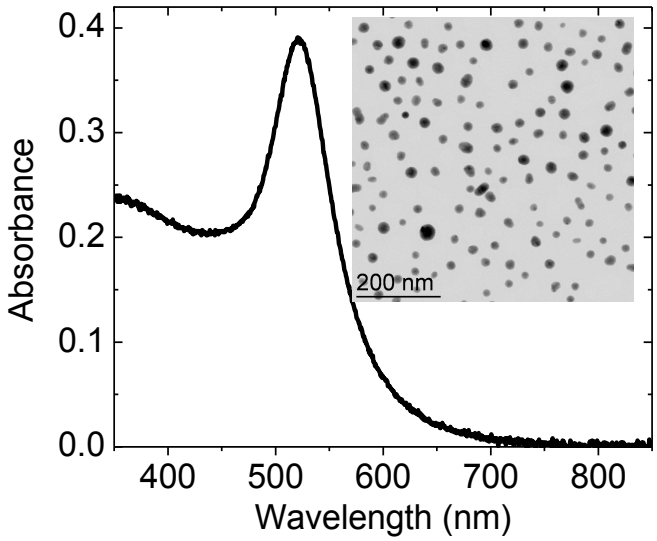

B

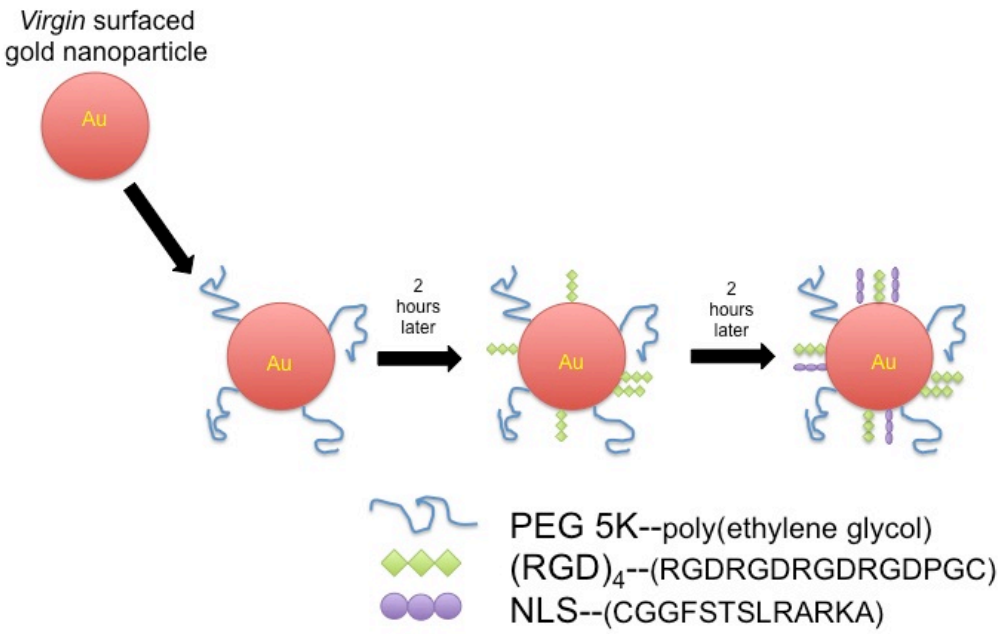

Figure 3.2: (A) Representative UV-VIS absorption spectrum of colloidal gold nanoparticles prepared by femtosecond laser ablation and a transmission electron microscopy (TEM) picture of these colloidal gold nanoparticles is shown

in the inset [21]. (B) Schematic of the sequential conjugation methods utilized to modify the surfaces of the nanoparticles.

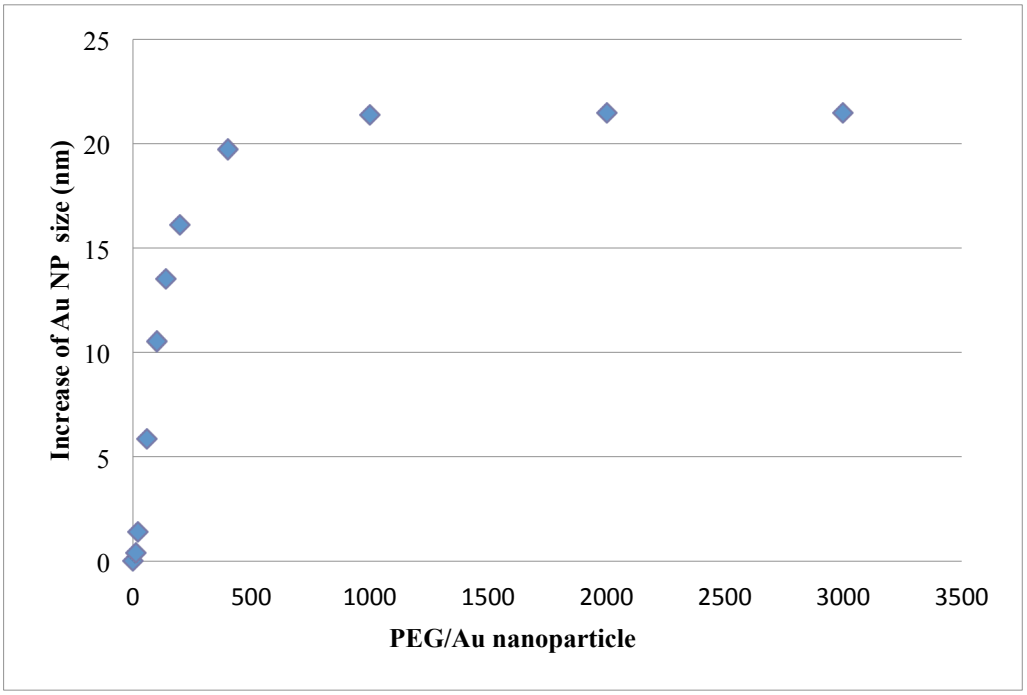

Figure 3.3: Experimental determination of the amount of thiolated PEG 5K required to form a complete monolayer on the surface of the femtosecond laser generated gold nanoparticle. Size increase of the nanoparticle as increasing concentrations of PEG 5K was added to the surface was determined using Dynamic Light scattering. The increase in nanoparticle size as compared to unmodified gold nanoparticles is shown here.

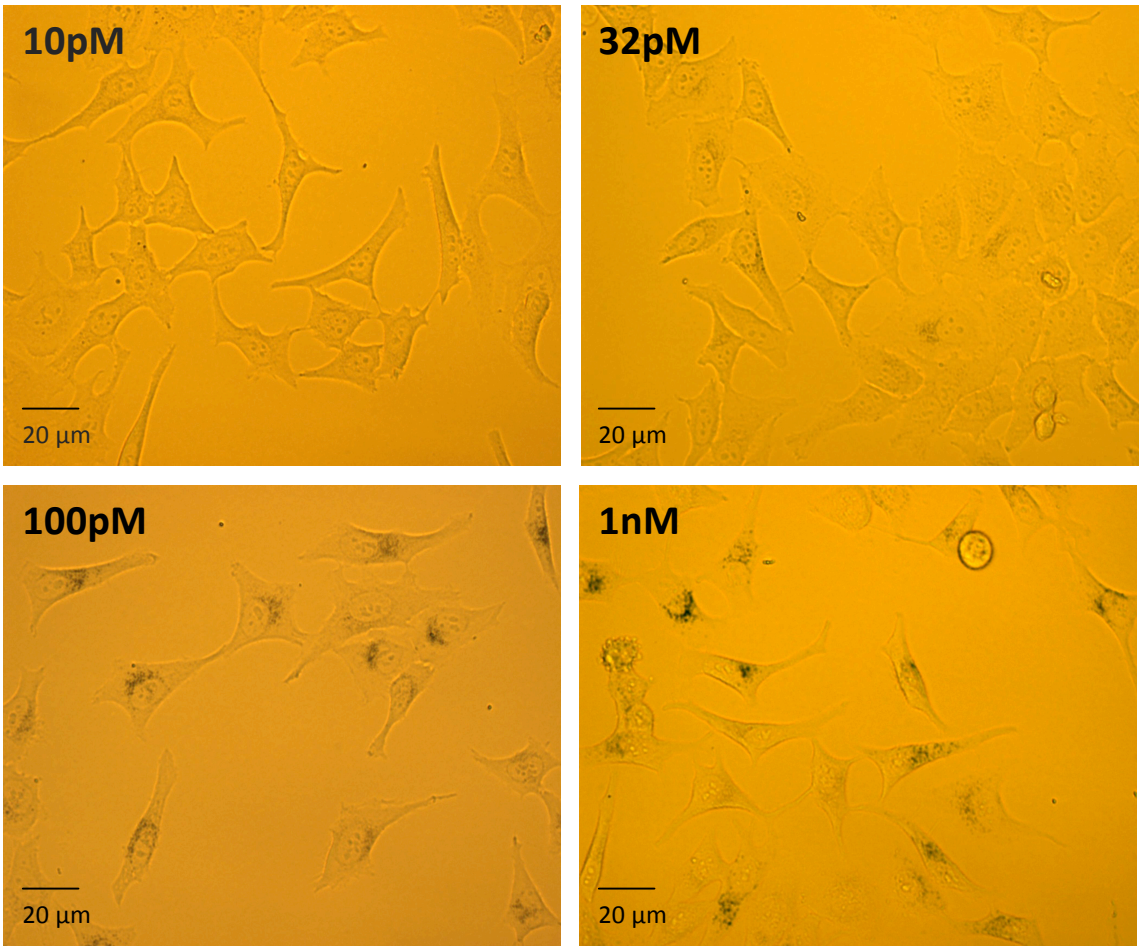

Figure 3.4: Bright field images of cancer cells that were incubated for 24 hours with varying concentrations of gold nanoparticles surface modified with molar ratios of 150 PEG 5K & 1000 RGD per nanoparticle.

A

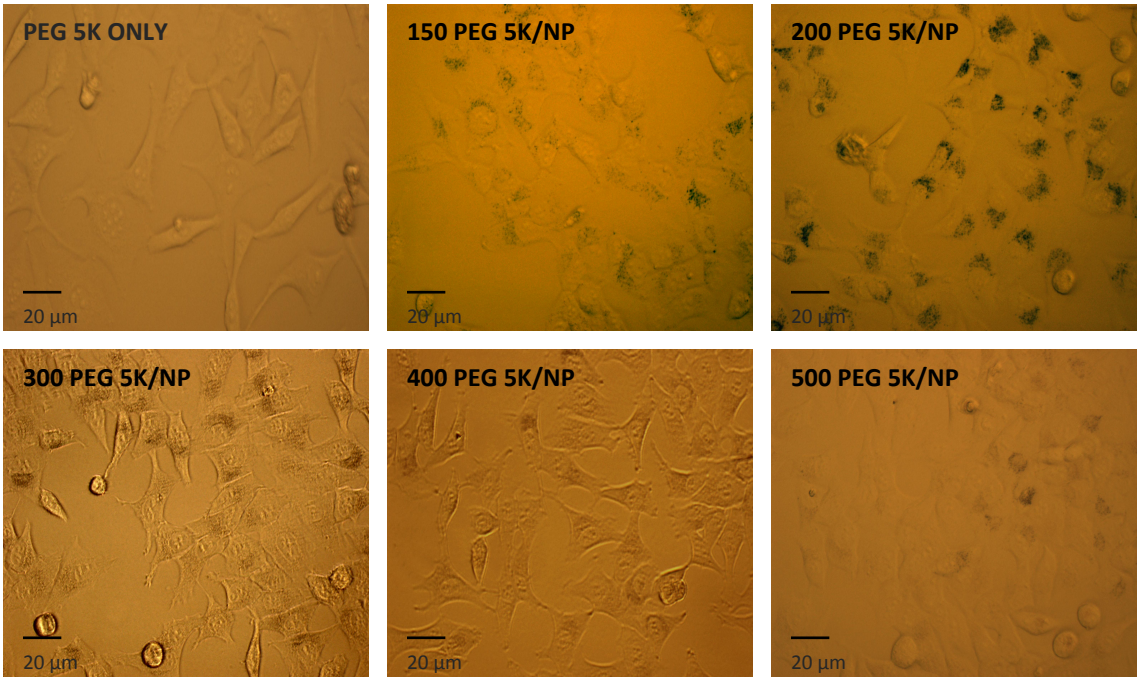
PEG 5K ONLY
20 µm
150 PEG 5K/NP
20 µm
200 PEG 5K/NP
20 µm
300 PEG 5K/NP
20 µm
400 PEG 5K/NP
20 µm
500 PEG 5K/NP
20 µm

B

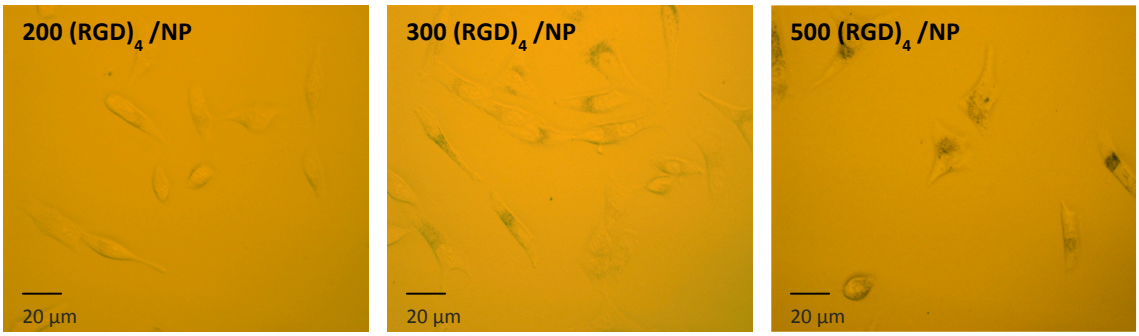
200 (RGD)4 /NP
20 µm
300 (RGD)4 /NP
20 µm
500 (RGD)4 /NP
20 µm

C

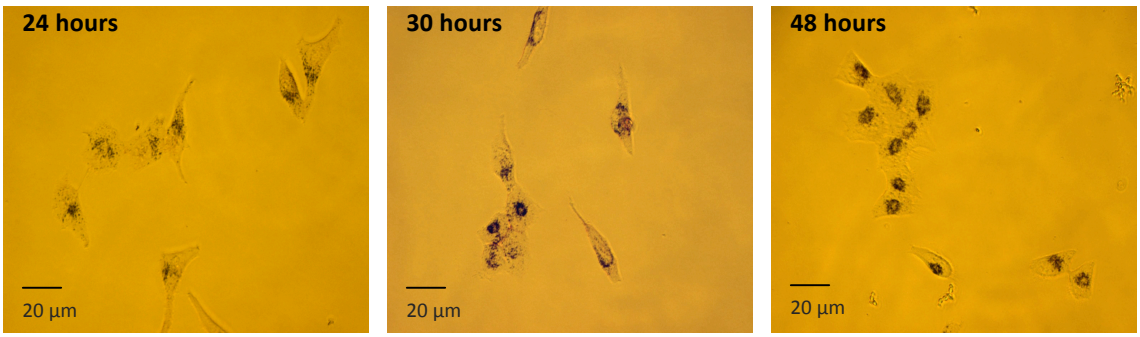
24 hours
20 µm
30 hours
20 µm
48 hours
20 µm

Figure 3.5: Bright field images of cancer cells. (3A) Cells that were incubated with surface modified gold NPs with varying molar ratios of PEG 5K per nanoparticle. (3B) Cells that were incubated with surface modified gold NPs with a molar ratio of 200 PEG 5K per nanoparticle and varying molar ratios of $(RGD)_4$ per nanoparticle. (3C) Cells that were incubated for varying times with gold nanoparticles that were sequentially conjugated with molar ratios of 200, 400, & 800 Of PEG 5K, $(RGD)_4$, and NLS, respectively.

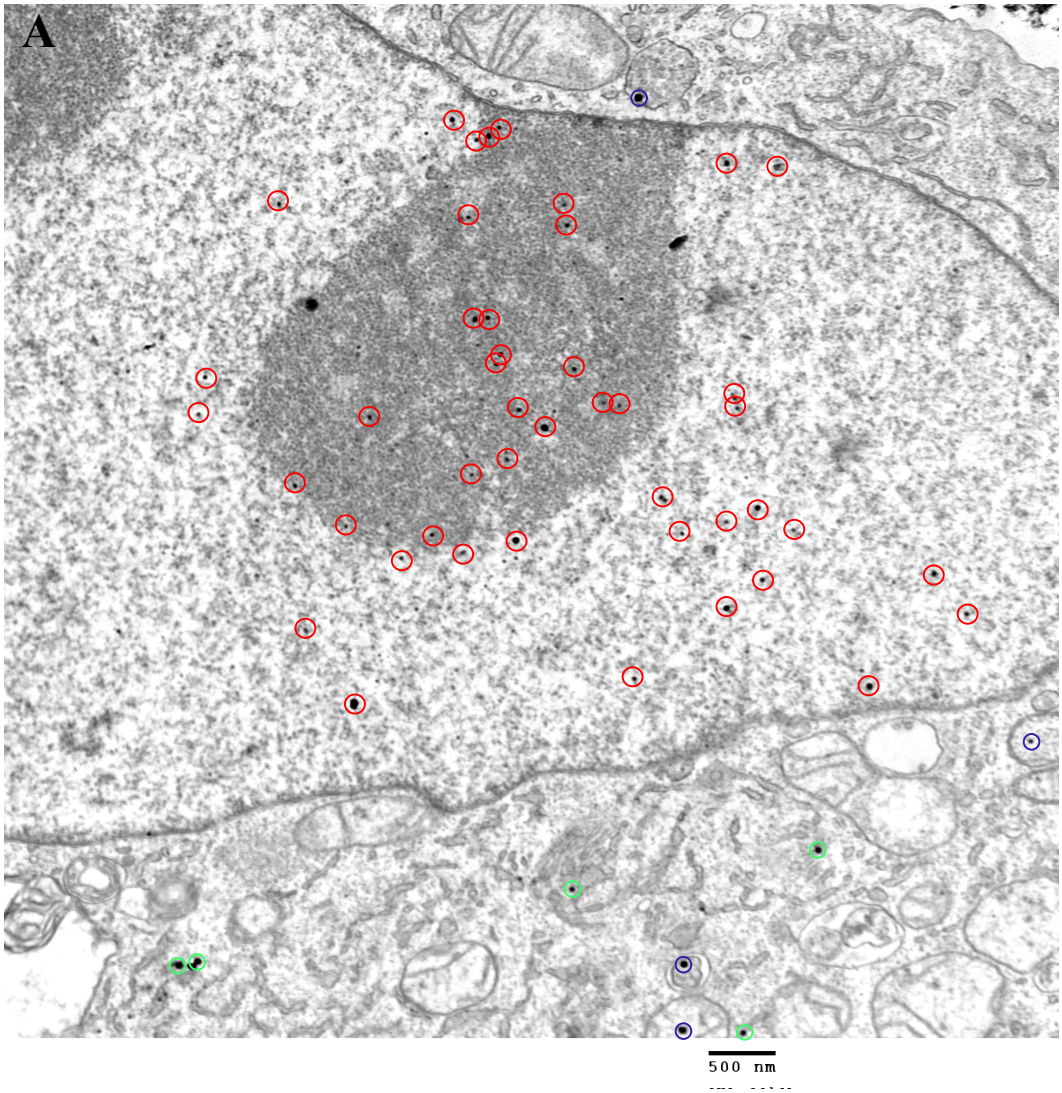
A
500 nm

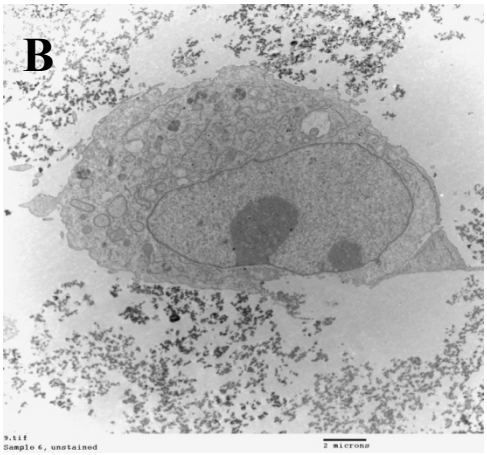
B
9.tif
Sample 6, unstained
2 microns

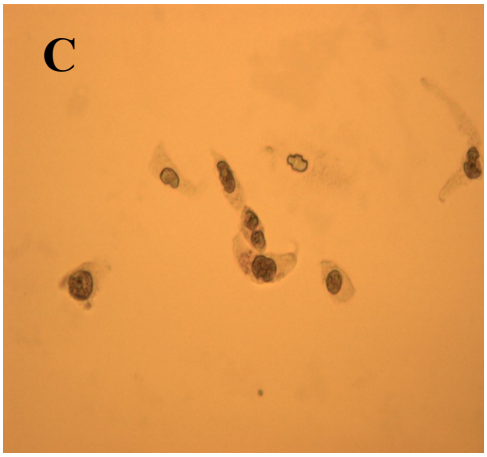
C

Figure 3.6: TEM Confirmation of nuclear delivery. (A) Surface modified gold nanoparticles inside of the cell's nucleus are denoted by red circles. Gold nanoparticles located in the cytosol (circled in green) and within the lysosome/endosome complex (circled in blue) are also noted. (B) Zoomed out view of the same cancer cell. (C) Bright field image of cells before they were fixed.

3.8 References:

1. Jain, P. K.; Huang, X. H.; El-Sayed, I. H.; El-Sayed, M. A., Noble Metals on the Nanoscale: Optical and Photothermal Properties and Some Applications in Imaging, Sensing, Biology, and Medicine. *Accounts of Chemical Research* **2008,** *41* (12), 1578-1586.

2. Copland, J. A.; Eghtedari, M.; Popov, V. L.; Kotov, N.; Mamedova, N.; Motamedi, M.; Oraevsky, A. A., Bioconjugated gold nanoparticles as a molecular based contrast agent: Implications for imaging of deep tumors using optoacoustic tomography. *Molecular Imaging and Biology* **2004,** *6* (5), 341-349;

3. Boisselier, E.; Astruc, D., Gold nanoparticles in nanomedicine: preparations, imaging, diagnostics, therapies and toxicity. *Chemical Society Reviews* **2009,** *38* (6), 1759-1782.

4. Chithrani, Intracellular uptake, transport, and processing of nanostructures in cancer cells. 2009.

5. Popovtzer, R.; Agrawal, A.; Kotov, N. A.; Popovtzer, A.; Balter, J.; Carey, T. E.; Kopelman, R., Targeted Gold Nanoparticles Enable Molecular CT Imaging of Cancer. *Nano Letters* **2008,** *8* (12), 4593-4596.

6. Huang, X. H.; El-Sayed, I. H.; Qian, W.; El-Sayed, M. A., Cancer cell imaging and photothermal therapy in the near-infrared region by using gold nanorods. *Journal of the American Chemical Society* **2006,** *128* (6), 2115-2120.

7. Huang, H. C.; Barua, S.; Sharma, G.; Dey, S. K.; Rege, K., Inorganic nanoparticles for cancer imaging and therapy. *Journal of Controlled Release* **2011,** *155* (3), 344-357.

8. Wang, L. S.; Chuang, M. C.; Ho, J. A. A., Nanotheranostics - a review of recent publications. *International Journal of Nanomedicine* **2012,** *7*, 4679-4695.

9. Skrabalak, S. E.; Chen, J.; Au, L.; Lu, X.; Li, X.; Xia, Y. N., Gold nanocages for biomedical applications. *Advanced Materials* **2007,** *19* (20), 3177-3184.

10. Letfullin, R. R.; Joenathan, C.; George, T. F.; Zharov, V. P., Laser-induced explosion of gold nanoparticles: potential role for nanophotothermolysis of cancer. *Nanomedicine* **2006,** *1* (4), 473-480.

11. Li, W. Y.; Brown, P. K.; Wang, L. H. V.; Xia, Y. N., Gold nanocages as contrast agents for photoacoustic imaging. *Contrast Media & Molecular Imaging* **2011,** *6* (5), 370-377.

12. Coulter, J. A.; Jain, S.; Butterworth, K. T.; Taggart, L. E.; Dickson, G. R.; McMahon, S. J.; Hyland, W. B.; Muir, M. F.; Trainor, C.; Hounsell, A. R.; O'Sullivan, J. M.; Schettino, G.; Currell, F. J.; Hirst, D. G.; Prise, K. M., Cell type-dependent uptake, localization, and cytotoxicity of 1.9 nm gold nanoparticles. *International Journal of Nanomedicine* **2012,** *7*, 2673-2685.

13. Dworetzky, S. I.; Lanford, R. E.; Feldherr, C. M., The effects of variations in the number and sequence of targeting signals on nuclear uptake. *Journal of Cell Biology* **1988,** *107* (4), 1279-1287.

14. Nativo, P.; Prior, I. A.; Brust, M., Uptake and intracellular fate of surface-modified gold nanoparticles. *Acs Nano* **2008,** *2* (8), 1639-1644.

15. Hah, H. J.; Kim, G.; Lee, Y.-E. K.; Orringer, D. A.; Sagher, O.; Philbert, M. A.; Kopelman, R., Methylene Blue-Conjugated Hydrogel Nanoparticles and

Tumor-Cell Targeted Photodynamic Therapy. *Macromolecular Bioscience* **2011,** *11* (1).

16. Lee, Y.-E. K.; Ulbrich, E. E.; Kim, G.; Hah, H.; Strollo, C.; Fan, W.; Gurjar, R.; Koo, S. M.; Kopelman, R., Near Infrared Luminescent Oxygen Nanosensors with Nanoparticle Matrix Tailored Sensitivity. *Analytical Chemistry* **2010,** *82* (20), 8446-8455.

17. Lee, Y. E. K.; Kopelman, R., Targeted, Multifunctional Hydrogel Nanoparticles for Imaging and Treatment of Cancer. *Multifunctional Nanoparticles for Drug Delivery Applications: Imaging, Targeting, and Delivery* **2012**, 225-255.

18. Nie, G. C.; Hah, H. J.; Kim, G.; Lee, Y. E. K.; Qin, M.; Ratani, T. S.; Fotiadis, P.; Miller, A.; Kochi, A.; Gao, D.; Chen, T.; Orringer, D. A.; Sagher, O.; Philbert, M. A.; Kopelman, R., Hydrogel Nanoparticles with Covalently Linked Coomassie Blue for Brain Tumor Delineation Visible to the Surgeon. *Small* **2012,** *8* (6), 884-891.

19. Reddy, G. R.; Bhojani, M. S.; McConville, P.; Moody, J.; Moffat, B. A.; Hall, D. E.; Kim, G.; Koo, Y. E. L.; Woolliscroft, M. J.; Sugai, J. V.; Johnson, T. D.; Philbert, M. A.; Kopelman, R.; Rehemtulla, A.; Ross, B. D., Vascular targeted nanoparticles for imaging and treatment of brain tumors. *Clinical Cancer Research* **2006,** *12* (22), 6677-6686.

20. Tkachenko, A. G.; Xie, H.; Coleman, D.; Glomm, W.; Ryan, J.; Anderson, M. F.; Franzen, S.; Feldheim, D. L., Multifunctional gold nanoparticle-peptide

complexes for nuclear targeting. *Journal of the American Chemical Society* **2003,** *125* (16), 4700-4701.

20. Krpetic, Z.; Saleemi, S.; Prior, I. A.; See, V.; Qureshi, R.; Brust, M., Negotiation of Intracellular Membrane Barriers by TAT-Modified Gold Nanoparticles. *Acs Nano* **2011,** *5* (6), 5195-5201.

21. Qian, W.; Murakami, M.; Ichikawa, Y.; Che, Y., Highly Efficient and Controllable PEGylation of Gold Nanoparticles Prepared by Femtosecond Laser Ablation in Water. *Journal of Physical Chemistry C* **2011,** *115* (47), 23293-23298.

22. Fojtik, A.; Henglein, A., Laser ablation of films and suspendend particles in a solvent - formation of cluster and colloid solutions. *Berichte Der Bunsen-Gesellschaft-Physical Chemistry Chemical Physics* **1993,** *97* (2), 252-254.

23. Fojtik, A.; Giersig, M.; Henglein, A., Formation of nanometer-size silicon particles in a laser-induced plasma inSiH4. *Berichte Der Bunsen-Gesellschaft-Physical Chemistry Chemical Physics* **1993,** *97* (11), 1493-1496.

24. Neddersen, J.; Chumanov, G.; Cotton, T. M., Laser-ablation of Metals - a new method for preparing SERS active colloids. *Applied Spectroscopy* **1993,** *47* (12), 1959-1964.

25. Liu, X.; Du, D.; Mourou, G., Laser ablation and micromachining with ultrashort laser pulses. *Ieee Journal of Quantum Electronics* **1997,** *33* (10), 1706-1716.

26. Weisbecker, C. S.; Merritt, M. V.; Whitesides, G. M., Molecular self-assembly of aliphatic thiols on gold colloids. *Langmuir* **1996,** *12* (16), 3763-3772.

27. Bellino, M. G.; Calvo, E. J.; Gordillo, G., Adsorption kinetics of charged thiols on gold nanoparticles. *Physical Chemistry Chemical Physics* **2004,** *6* (2), 424-428.

28. Di Felice, R.; Selloni, A., Adsorption modes of cysteine on Au(111): Thiolate, amino-thiolate, disulfide. *Journal of Chemical Physics* **2004,** *120* (10), 4906-4914.

29. Dam, D. H. M.; Lee, J. H.; Sisco, P. N.; Co, D. T.; Zhang, M.; Wasielewski, M. R.; Odom, T. W., Direct Observation of Nanoparticle-Cancer Cell Nucleus Interactions. *Acs Nano* **2012,** *6* (4), 3318-3326.

30. Oyelere, A. K.; Chen, P. C.; Huang, X. H.; El-Sayed, I. H.; El-Sayed, M. A., Peptide-conjugated gold nanorods for nuclear targeting. *Bioconjugate Chemistry* **2007,** *18* (5), 1490-1497.

31. Xie, J.; Xu, C.; Kohler, N.; Hou, Y.; Sun, S., Controlled PEGylation of monodisperse Fe3O4 nanoparticles for reduced non-specific uptake by macrophage cells. *Advanced Materials* **2007,** *19* (20), 3163-+.

32. Daou, T. J.; Li, L.; Reiss, P.; Josserand, V.; Texier, I., Effect of Poly(ethylene glycol) Length on the in Vivo Behavior of Coated Quantum Dots. *Langmuir* **2009,** *25* (5), 3040-3044.

33. Koo, Y. E. L.; Reddy, G. R.; Bhojani, M.; Schneider, R.; Philbert, M. A.; Rehemtulla, A.; Ross, B. D.; Kopelman, R., Brain cancer diagnosis and therapy with nanoplatforms. *Advanced Drug Delivery Reviews* **2006,** *58* (14), 1556-1577.

34. Tkachenko, A. G.; Xie, H.; Liu, Y. L.; Coleman, D.; Ryan, J.; Glomm, W. R.; Shipton, M. K.; Franzen, S.; Feldheim, D. L., Cellular trajectories of peptide-

modified gold particle complexes: Comparison of nuclear localization signals and peptide transduction domains. *Bioconjugate Chemistry* **2004,** *15* (3), 482-490.

Chapter 4 Optimization of Photothermal Therapy of Cancer Cells via Nuclear Delivery of Surface Modified Au Nanoparticles

4.1 Introduction

Gold is consistently used in various forms of nanoparticle-mediated therapy because of the ease of fabrication and surface modification, as well as gold's inherent biological compatibility [1-6] . Using simple wet lab techniques, gold nanoparticles have been fabricated in a variety of shapes and sizes, and used as the core or the shell for polymer/metal[2,3] and metal/metal[4,5] hybrid nanoparticles. One conventional method of fabricating gold nanoparticles involves citrate reduction of the +3 oxidized state of gold [6] mainly because no extra surfactants or polymers are needed to stabilize the gold nanoparticles[7]. Dyes, drugs, genetic materials, and targeting moieties can all be attached to gold nanoparticle surface directly via amine of thiol groups or indirectly using another molecule like bovine serum albumin (BSA)[8] or the pentapeptide with the amino acid sequence CALNN[9]. The ability to attach multiple types of ligand to the gold nanoparticle surface has led to varying schemes for developing multifunctional gold nanoparticles with multiple capabilities within a single platform [1,10,2]. Compared to other methods, treatment plans involving the use of multifunctional nanoparticles hold the promise of offering a more acutely targeted treatment with a higher likelihood of a successful outcome. In many studies, gold nanoparticles

have been utilized for drug delivery, therapy administration, and as a contrast enhancing agent for imaging applications. It is this multi-prong approach on which many research studies have anchored their treatment efficacy, since it addresses many issues usually associated with the most aggressive diseases including multidrug resistance and reoccurrence of tumors.

Gold nanoparticles have been most frequently exploited for photothermal therapy, in comparison to options such as metal, dye/polymer, or carbon-based nanoparticles. The exceptionally high extinction coefficient of gold ($1 \times 10^{19}\ M^{-1}\ cm^{-1}$ for 20 nm gold nanoparticles)[7] is orders of magnitude higher than that of strongly absorbing organic dyes (e.g. Coomassie blue, $4.3 \times 10^{4}\ M^{-1}\ cm^{-1}$) [11], which makes it an ideal photosensitizer. The localized surface plasmon resonance of gold nanoparticles is highly dependent on the morphology of the nanoparticles and can be easily tuned during the fabrication process [7]. Taken together, these two attributes have contributed significantly to the popularity of gold nanoparticles in facilitating photothermal therapy. To date, various cancer cell lines, including breast[12], epithelial [13,14] and colon[10] cancers, have been successfully treated by gold nanoparticle mediated photothermal therapy, both *in vitro* and *in vivo*. Studies involving photothermal therapy on antibiotic resistant bacteria[15,16] have also been reported with positive results.

This chapter describes a comparative study of photothermal therapy, contrasting treatment mediated by gold nanoparticles located predominately within the nucleus in to when the gold nanoparticles are predominantly in the cytoplasm. Building on the successful nuclear delivery of gold nanoparticles

described in the last chapter, the differences in efficacy due to nanoparticle location, treatment time, and nanoparticle concentration were studied. The gold nanoparticles utilized in these studies were surface engineered, either with a combination of PEG 5K and $(RGD)_4$ peptide (intracellular delivery predominantly to the cytoplasm) or of PEG 5K, $(RGD)_4$ (RGDRGDRGDRGDPGC), and NLS(CGGFSTSLRARKA) peptides for nuclear delivery. The motivation for this study is to investigate the likely advantages of directly heating the nucleus of cancer cells, advantages stemming from the fact that the nucleus has a smaller target volume, a lower heat capacity, and an increased likelihood of causing irreparable damage to the cell's DNA. Furthermore, it is likely that some nucleus specific PTT will induce notable differences in the mechanisms through which the cancer cell dies, which will provide invaluable insight for *in vivo* treatment planning.

4.2 Theoretical background

Photothermal therapy involves the irradiation of a photosensitizer to generate heat so as to damage the region of interest. The photosensitizer absorbs the incoming irradiation and, subsequently, the electrons are excited from the ground state to a higher energy state. Heat is produced in the sample through the non-radiative de-excitation of the electrons from the upper state to the ground state. The utility of a particular photosensitizer can be characterized exclusively by the amount of heat generated and the resulting temperature increase when the photosensitizer is illuminated at the exciting wavelength. The

amount of energy absorbed by the photosensitizer, Q_{abs}, following light irradiation, is given by the following equation [17]

$$Q_{abs} = S_{es} \int_0^t I_0(t) K_{abs}\, dt \qquad \text{Equation 4.1}$$

where S_{es} is the surface area of a spherical equivolume gold nanoparticle being illuminated for a time *t*, given by the equation

$$S_{es} = \pi r_{es}^2, \qquad \text{Equation 4.2}$$

Where r_{es} is the radius of the equivolume gold sphere,

$$V_0 = \frac{4}{3}\pi r_a r_b^2, \qquad r_{es} = (r_a\, r_b^2)^{\frac{1}{3}} \qquad \text{Equations 4.3 \& 4.4}$$

$r_a = r_b$ in our case of gold spheres. K_{abs}, is the absorption efficiency factor, defined as the absorption coefficient, α_{abs}, divided by the area of the nanoparticle being illuminated

$$K_{abs} = \frac{a_{abs}}{\pi r_{es}^2} \qquad \text{Equation 4.5}$$

and $I_0(t)$ is the incident light intensity given as a function of time *t*. Using the coefficient of absorption, α_{abs}, Equation 4.1 can be rewritten in a more familiar form [17]:

$$Q_{abs} = \int_0^t \alpha_{abs}\, I_0(t)\, dt$$ Equation 4.6

The thermal energy (E_T) of the system, after light irradiation of the gold nanoparticle, is given by the equation:

$$E_T = mCT$$ Equation 4.7

m, *C,* and *T* denote the mass, specific heat and temperature, respectively. Using energy conservation,

$$Q_{abs} = E_T - E_0 - Q_m$$ Equation 4.8

where E_T, E_0, and Q_m is the final energy, initial energy, and energy spent toward the melting of the nanoparticle, respectively. When all of the absorbed energy goes toward generating heat and not melting, as in our case, the change in temperature is given by[17]

$$\Delta T = \frac{Q_{abs}}{\rho CV}$$ Equation 4.9

where ρ is the density of gold and V is the volume of the nanoparticle. To estimate the temperature change in the present study, we must take into account that the gold nanoparticles are illuminated using a laser. To estimate Q_{abs} the experimental value of the energy absorbed by the gold nanoparticle per mass [18] (approximately 2 X 10^3 J g^{-1} $pulse^{-1}$) is used. Plugging in the parameters for the

nanoparticles used in the present study, ($r = 10^{-6}$ cm) yields a ΔT on the order of 10^3. This value is comparable to the both theoretical[19] and experimental[18] values previously reported. However, the energy lost to the surrounding, in this case, the cancer cell, must be taken into account as the long excitation time (~μs) enables conductive/convective heat loss. The estimated heat loss for a gold nanoparticle of this size occurs over a much shorter time span (4.5×10^{-17} J per particle per 7 ns)[18]. Further, the confocal microscope scans across all of the pixels in the treatment area every 2.54s. This scan time likely allows the complete cooling of the nanoparticle between successive excitations, thus it is estimated that the temperature increase is less than 10% of the predicted value.

4.3 Materials & Methods

4.3.1 Materials

Dulbecco's Modified Eagle medium (DMEM 1195 & 21063), Dulbecco's Phosphate Buffered Saline (DPBS), fetal bovine serum (FBS), penicillin-streptomycin glutamine, and the Live/Dead *Bac*light Bacterial Viability Kit were all purchased from Invitrogen. 100mm and 35mm Petri dishes were purchased from BD Biosciences. 8 well, chambered plates were purchased from Fisher Scientific. Thiolated poly(ethlylene glycol) with a molecular weight of 5 kiloDaltons was purchased from Nancos (New York, NY). Rectangular gold target (16mm long, 8mm wide, 0.5mm thick) was purchased from Alfa Aesar. $(RGD)_4$ and NLS peptides were purchased from RS Synthesis (Louisville, KY). The water used

throughout the experiment was de-ionized (DI) water, purified by a Milli-Q system from Millipore Co.

4.3.2 Cell culture

HeLa 229 cells (American Type Culture Collection) were grown in Dulbecco's modified Eagle medium (DMEM 11995) supplemented with 10% fetal bovine serum (FBS) and 1% penicillin-streptomycin at 37°C and 5% CO_2 in a humidified incubator. Cells were plated and grown in 8 well borosilicate chambered plates (Fisher Scientific) for all of the PTT experiments.

4.3.3 Nanoparticle Characterization & Surface Modification

All gold nanoparticles utilized for the photothermal therapy described in this chapter were fabricated using femtosecond laser ablation, as described in the previous chapter. The nanoparticles' physical "virgin surface" and absorbance are identical to those of the last chapter, however, the average diameter and size distribution was slightly higher, with an average diameter of 30, as measured by dynamic light scattering. The gold nanoparticles were also imaged on the TEM to verify the average diameter and size distribution. The DLS information and TEM images of the gold nanoparticles are shown in Figure 4.1.

In an effort to utilize the extra surface area of these larger nanoparticles, the amounts of stabilizing and targeting moieties used for modifying the surface of the nanoparticles were increased from those used in the previous chapter to

the following molar ratios: PEG 5K -- 200/per nanoparticle, $(RGD)_4$ — 500/per nanoparticle, and NLS - 800/per nanoparticle.

The temperature change of the gold nanoparticle solution during illumination was measured in the following way. Solutions of 100pM, 500pM, and 1nM concentration of gold nanoparticles dissolved in growth media were placed inside of eight well plates in the onstage incubator; the temperature of the solutions was allowed to equilibrate between 36.5-38.5°C. A thermocouple was placed in the well, directly above the objective, so that the temperature of the solution being irradiated could be measured. The temperature was recorded every 5 minutes (including before illumination), up to 40 minutes. Cell media with no nanoparticles were also illuminated as a control. The change in temperature (ΔT) was calculate by substrating the temperature at a time t, T_t, from the initial temperature of the sample before illumination, T_0. The very slight temperature changes of the solutions are shown in Figure 4.2.

4.3.4 Imaging/Live-dead Assay

After incubation with the gold nanoparticles, cells were washed three times with HBSS to remove any nanoparticles remaining outside of the cells, and new clear growth media was added (DMEM 21063). 2μL of 1.5 mM of Propidium Iodide dissolved in DMSO and 1μL of 2 mM of Calcein AM dissolved in DMSO were added to the cells and allowed to incubate for at least 10 minutes. The cells were kept at biological temperatures throughout the experiment, inside an on-stage incubator, with temperatures ranging from 36.5-38.5°C, as monitored by

a thermocouple. All images used to quantify the efficacy of the PTT were performed on a Leica SP5X inverted confocal microscope system (Leica Microsystems, USA), using a 20x objective. Three images were taken simultaneously; one image was taken for each dye's emission and a third image was taken using differential interference contrast (DIC). An example of the 3 images taken at each time point is shown in Figure 4.3. The images were analyzed using the Leica software; the number of live cells, indicated with the presence of Calcein AM fluorescence, and of dead cells, indicated by propidium iodide fluorescence, in the nucleus, was calculated for various time points.

4.3.5 Photothermal Therapy (PTT)

All PTT experiments were performed on a Leica SP5X inverted confocal microscope system (Leica Microsystems, USA). The cells were first imaged before treatment, so as to establish a baseline. The cells were then illuminated with an argon laser (excitation 514nm), focused through a 20X objective to a spot size of .575 μm^2. The power at the sample was measured to be 3.87mW. The treatment area was .602mm^2. The microscope was set to scan throughout this area at a rate of 400Hz, giving a fluence of 1.64 J/cm^2 during the PTT treatments.

4.3.5a Short-term experiments

Short-term PTT experiments were conducted in which cells that had been previously incubated with varying concentrations of gold nanoparticles (between 100pm-1nM, with and without NLS) were treated for either 30 or 40 minutes.

The cells were imaged immediately before and after treatment, and then every 45 minutes, for up to 3 hours. Short-term experiments, with 30 minutes of PTT treatment, were conducted in duplicates, and the short-term experiments with 40 minutes of PTT were conducted in triplicates.

4.3.5b Long-term experiments

To investigate if cells continue to die after the initial 3 hours of observation, for the short-term studies, another set of experiments was conducted in which the cells previously incubated with varying concentrations of gold nanoparticles (between 100pm-1nM, with and without NLS) were illuminated for 40 minutes. The cells were imaged immediately before and after treatment. Another set of images were taken right after treatment, and again at 6 hours and 12 hours post-treatment.

4.3.6 Controls

Controls were conducted to establish the absence of dark toxicity associated with the gold nanoparticles, as well as the absence of cell death due to light irradiation without the nanoparticles. The control cells without the gold nanoparticles were illuminated for 40 minutes, the maximum amount of time utilized for the PTT experiments. Cell survival was monitored, using the Live/Dead assay, for up to 12 hours after illumination. Also, cells that were previously incubated with 1nM of gold nanoparticles, for both 24 and 48 hours, were imaged for up to 12 hours, without any prolonged light exposure, to monitor their survival. In both cases, no cell death was observed, thus demonstrating that

any cell death observed with the gold-nanoparticle mediated PTT is due solely to internal heating, caused by the nanoparticles upon light irradiation.

4.3.7 Transmission Electron Microscopy

Samples that had been incubated with concentrations of 500pM and 1nM of gold nanoparticles for 48 hours, were washed 3 times, to remove any nanoparticle outside of the cells, and then fixed in 2.5 percent glutaraldehyde, in 0.1 M Sorensen's buffer, pH 7.4, overnight, at 4°C. After several buffer rinses, the cells were postfixed, using 1 % osmium tetroxide in buffer. The cells were then rinsed in doubly distilled water, to remove phosphate salt, and then en bloc stained with aqueous 3 % uranyl acetate, for one hour. The samples were dehydrated in ascending concentrations of ethanol, rinsed two times in 100% ethanol and embedded with epoxy resin. The samples were then ultra-thin sectioned into 70 nm slices and half of the samples were stained with uranyl acetate and lead citrate. The sections were then fixed onto TEM grids and imaged, to locate the presence of the gold nanoparticles throughout the cells.

4.4 Results & Discussion

There are clear differences in the patterns of cell death over time between the cells that were incubated and treated with gold nanoparticles modified with all three peptides and the cells that were incubated and treated with gold nanoparticles but modified with only PEG 5K and $(RGD)_4$.

4.4.1 Short-term studies

30 minutes PTT treatment: In all cases, whether the cells were incubated with gold nanoparticles that were modified with only PEG 5K and $(RGD)_4$ or had the PEG 5K, $(RGD)_4$, and NLS on the surface, 30 minutes of treatment did not yield complete cell death within the 3 hours of observation. In the case of gold nanoparticles with PEG 5K and $(RGD)_4$ only, the efficacy of treatment did increase with increasing nanoparticle concentration. There was very little to no cell death observed directly after these treatments, and approximately a 2.5, 6.5 and 8% decrease in the number of live cells was observed three hours post-treatment for 100pM, 500pm, and 1nM nanoparticle concentrations, respectively.

The efficacy of the PTT therapy on cells that were treated with gold nanoparticles that had NLS attached to them increased with increase in nanoparticle concentration from 100pM to 500pM; a decrease of approximately 25 and 50% in the number of live cells was observed after 3 hours post-treatment. Surprisingly when the nanoparticle concentration was further increased to 1nM, the efficacy decreased, yielding only an approximately 15% decrease in live cells, three hours post-treatment.

Although complete cell death was not observed for any cells treated for 30 minutes, we observed a difference in the way that the cells died after treatment with respect to the different types of surface modifications. The cells treated with the gold nanoparticles with only PEG and $(RGD)_4$ attached to the surface die slowly over time, reaching the maximum efficacy at the latest time point. On the other hand, cells treated with gold nanoparticles that have NLS peptide on the

surface experienced a majority cell death already within 45 minutes post treatment. The cells continued to die slowly over the rest of the observation time. All of these results are presented in Figure 4.4.

40 minutes PTT treatment: A significant increase in the PTT efficiency was observed for cells that were illuminated for 40 minutes following incubation with 500pM gold nanoparticles without NLS. Approximately an eight-fold increase was observed 3 hours post-treatment, in comparison to 30 minutes trials. In the experiment with 100pM, the efficacy of the PTT also increased, but only three times the efficacy associated with 30 minutes of PTT. Surprisingly, no change in the PTT efficiency was observed with the increase in treatment time for the cells incubated with the 1nM concentration of nanoparticles. The behavior of the cell viability curves did not change with the increase in treatment time.

The overall change in the percent of cells alive after three hours is strikingly different when the therapy is mediated by gold nanoparticles with NLS peptide. Nearly complete cell death was observed within 3 hours for cells incubated with 500pM. A 50% and 25% decrease in live cells was observed for cells incubated with 100pM and 1nM, respectively. Surprisingly, the combination of the largest nanoparticle concentration and treatment time (for gold nanoparticles with NLS) yielded a treatment efficacy comparable to the same nanoparticle concentration for gold nanoparticles without the NLS peptide. All of these results are presented in Figure 4.5.

4.4.2 Long-term studies

Longer observation periods were deemed necessary because, although the cells were still alive after 3 hours, the cells appeared to be damaged. As previously noted, a cell that fluoresced green was counted as alive, however morphological changes were observed by eye 3 hours post-treatement. We postulated that this damage could lead to death over a longer period of time, especially in the case of the cells treated with gold nanoparticles that had not been modified with NLS. The viability curves of those trials were still decreasing in time for all concentrations and treatment times, although very slightly in some cases.

As originally postulated, the cells that were treated with gold nanoparticles without NLS did continue to die over time (Figure 4.6). The maximum treatment efficacy was observed 12 hours post-treatment for cells treated with 100pM and 500pM, with 40-50% of the cells remaining alive. In contrast, complete cell death was observed within 6 hours for cells that were treated with all concentrations of gold nanoparticles with NLS.

4.4.3 Intracellular Nanoparticle Fate

Nuclear delivery of the nanoparticles was confirmed; Figures 7 & 8 are representative TEM images for 500pM and 1nM concentrations, respectively. The surprising decrease in cell death observed in the trials with 1nM of NLS modified gold nanoparticles is believed to be due to a decrease in the amount of gold nanoparticles able to achieve nuclear delivery. The increase in the

nanoparticles' concentration probably resulted in clumping/aggregation of the nanoparticles, thus barring them from passing through the nuclear pore. As shown in Figure 4.9, the gold nanoparticles inside of the cells that were treated with the highest nanoparticle concentration are seen to be compartmentalized in large clusters, although some free gold nanoparticles are also present. Trapped clusters were also observed in cells treated with 500pM; however, these clusters were usually smaller and less prevalent. Also, this observed clumping effect likely resulted in less efficient absorption and generation of heat throughout the cell since the aggregation of the nanoparticle would induce a shift in the localized surface plasmon resonance.

The differences in the viability curves of cells treated with NLS decorated gold nanoparticles, compared to cells treated with gold nanparticles without NLS, arises due to different intracellular heating locations within the cells at the time of irradiation. The nanoparticles that were not modified with NLS have no way of entering the nucleus. These nanoparticles are therefore either free in the cytosol or trapped within its compartments, at the time of light treatment. Heating due to this type of intracellular, spatial distribution is less effective in cell kill. We suspect that the local temperature rise due to the nanoparticles harm and maybe damages parts of the cell but results in a small number of cell death within 3 hours, as reflected in the slow decline seen in the viability curves. On the other hand, the nanoparticles modified with NLS have the ability to enter the nucleus. The presence of the nanoparticles in the nucleus enables direct heating of the DNA, probably causing irreparable damage and quick cell death, as reflected in

the sharp decrease seen in the viability curves and then a slow decrease toward complete cell death. One possible reason for this type of behavior is that across the entire sample there is some distribution in the number of gold nanoparticles inside each nucleus, as the number of nanoparticles within the nucleus depends on many factors. There is a threshold of heat needed to kill the cells within the first 45 minutes after treatment. The cells exposed to at least this threshold of heat at the time of treatment die immediately, while other cells are damaged but do not die within three hours. These cells do however sustain enough damage and die within 6 hours.

4.5 Conclusions

In the present study, a stark difference in treatment efficacy was observed when the PTT was mediated by gold nanoparticles within the nucleus compared to when the nanoparticles could not enter the nucleus. When the gold nanoparticles were modified to include NLS, a peptide that facilitates nuclear uptake, irreparable damage was caused and efficient cell death was observed for various concentrations, after 40 minutes of light irradiation. However, from our studies it becomes apparent that nuclear delivery is concentration dependent, because higher concentrations led to clumping within the cells, barring nuclear delivery. Thus, increasing the nanoparticle concentration did not improve the treatment efficacy as originally expected. It is possible that an increase in nanoparticle concentration yields a different biological response from the cells, resulting in sequestering of the intracellular gold, within cell compartments, in

large clumps. Although the intracellular nanoparticle concentration was probably higher for the highest nanoparticle concentration, the clumping of the gold nanoparticles seems to have resulted in a decrease in nuclear uptake. When the nanoparticles were not modified for nuclear uptake, the treatment efficacy was only improved significantly in the experiments involving 500pM nanoparticle concentrations, when observed over 3 hours, and all concentrations resulted in similar PTT efficacy after 12 hours. The clumping effect observed in the cells treated with NLS probably also occurred in those cells treated with nanoparticles without NLS, resulting in the lack of improvement despite the longer treatment times.

We observe that nuclear delivery of gold nanoparticles results in a stark difference in the outcomes of the photothermal therapy. The results of these studies further underline the great interest in nuclear targeting. We show that nuclear delivery enables a more effective therapy option as is also the case for various forms of therapy, including gene and photodynamic therapy[1].

4.6 Acknowledgements

I would like to acknowledge Sasha Meshinchi, Chris Edwards and the rest of the staff of Microscopy and Imaging Analysis Laboratory at the University of Michigan-Ann Arbor.

4.7 Figures

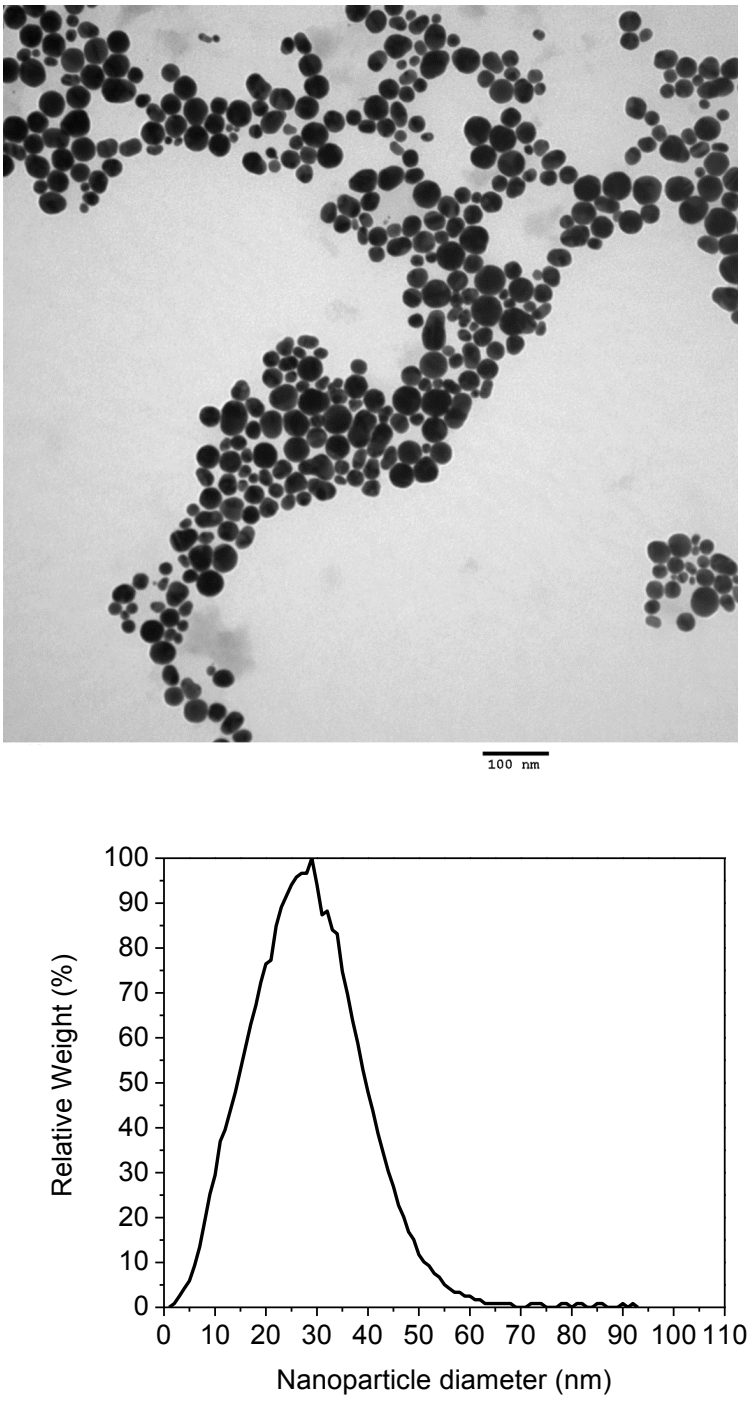

Figure 4.1: (Top) TEM image and (Bottom) dynamic light scattering data (DLS) of unmodified gold nanoparticles. Average diameter of the nanoparticles is 30nm.

Nanoparticle Concentration	No nanoparticles	100pM	500pM	1nM
Time (mins)	ΔT	ΔT	ΔT	ΔT
0	0	0	0	0
5	0.1	0.1	0.5	0.8
10	0.1	0.1	0.5	1
15	0	0.1	0.6	1.1
20	0.1	0.2	0.6	1.1
25	0.2	0	0.6	1.1
30	0.1	0.1	0.7	1.1
35	0.1	0.1	0.7	1.1
40	0.2	0.1	0.7	1

Figure 4.2: Temperature change of gold nanoparticles dissolved in cell media and illuminated continuously for 40 minutes. Starting temperature was in the biological range. Cell media was also illuminated as a control.

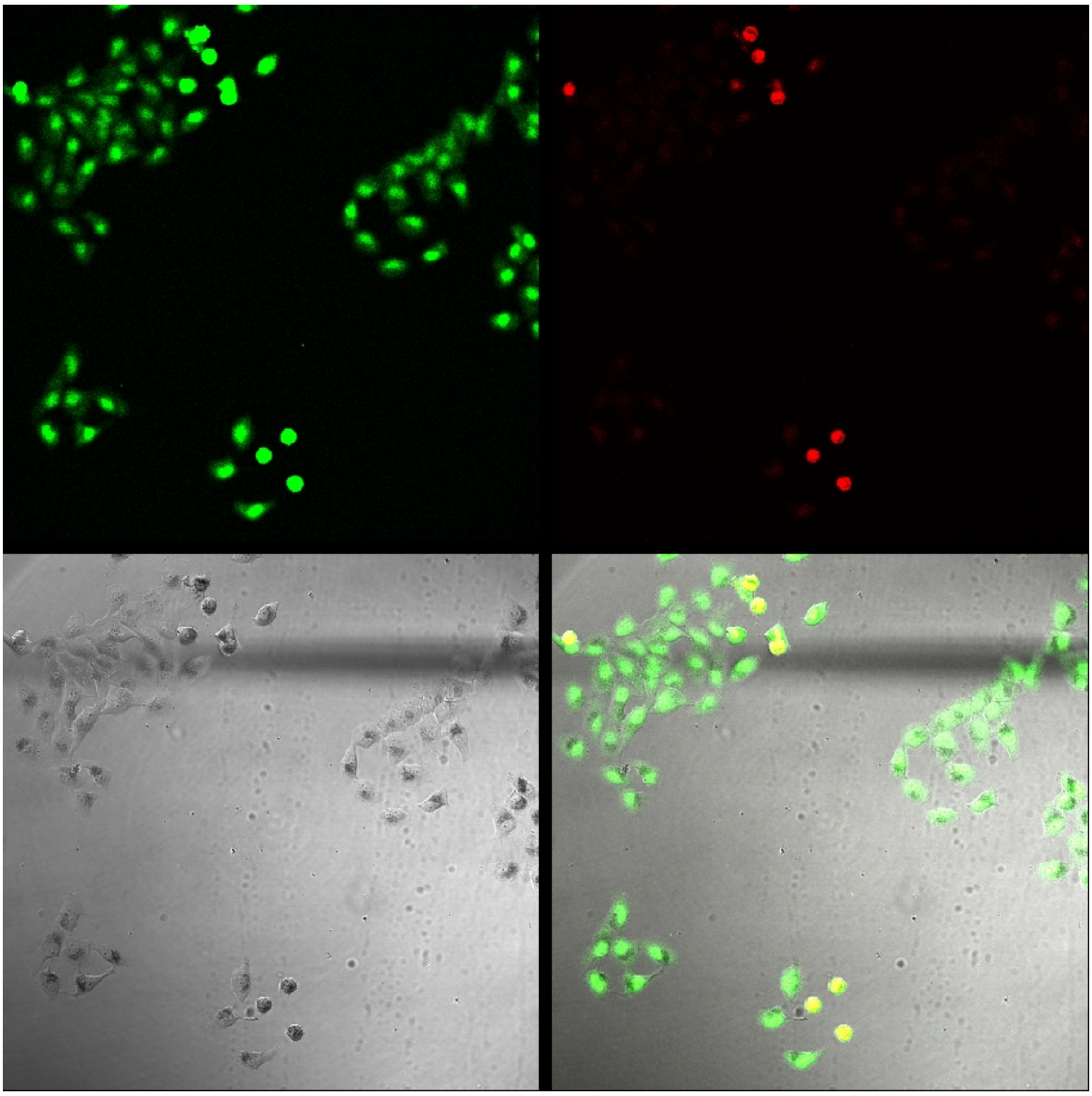

Figure 4.3: Representative images and composite image of Live/Dead assay utilized to characterized the efficacy of treatment. Top left: calcein channel (em. 510-520nm), top right: propidium iodide channel (em. 612-622), bottom left: DIC image, bottom right: composite image.

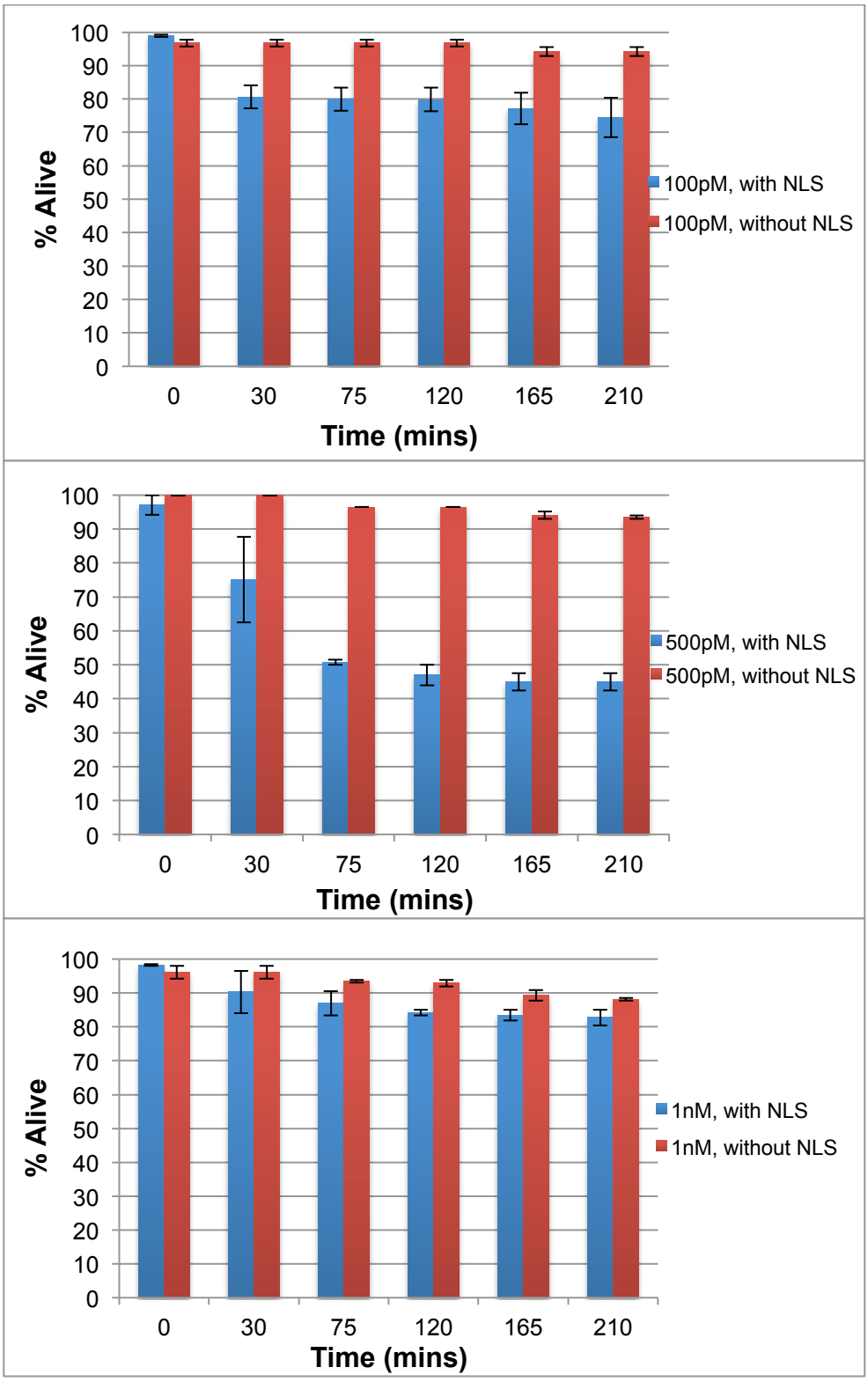

Figure 4.4: Viability of cells incubated with varying concentrations of gold nanoparticles modified with either PEG 5K, $(RGD)_4$ only or PEG 5K, $(RGD)_4$ with

and NLS and then illuminated at 514nm for 30 minutes. All experiments were done in duplicates. Error bars denote standard error in the percent of live cells at a given time point.

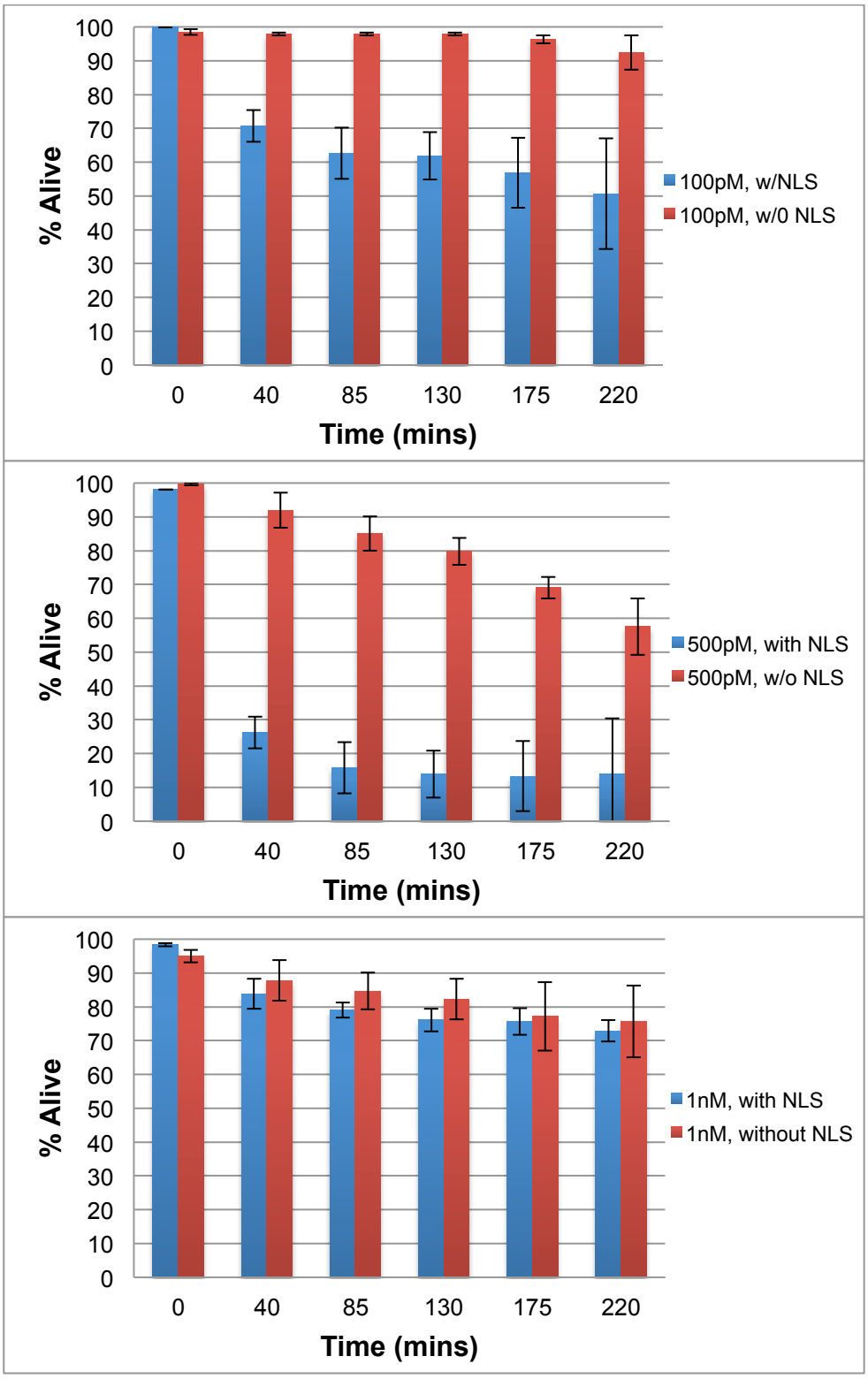

Figure 4.5: Viability of cells incubated with varying concentrations of gold nanoparticles modified with either PEG 5K, $(RGD)_4$ only or PEG 5K, $(RGD)_4$ with

and NLS and then illuminated at 514nm for 30 minutes. All experiments were done in triplicates. Error bars denote standard error in the percent of live cells at a given time point.

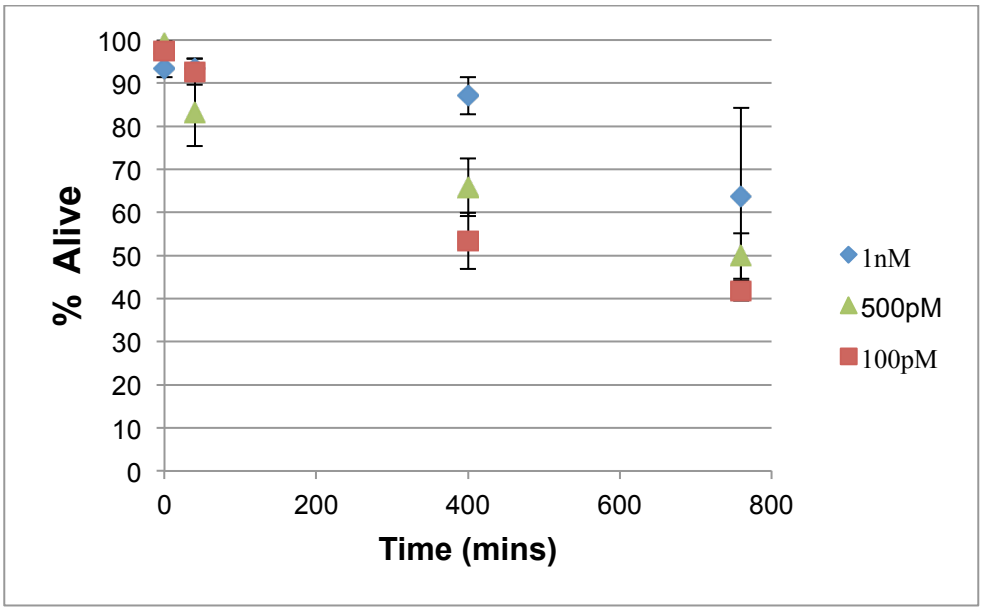

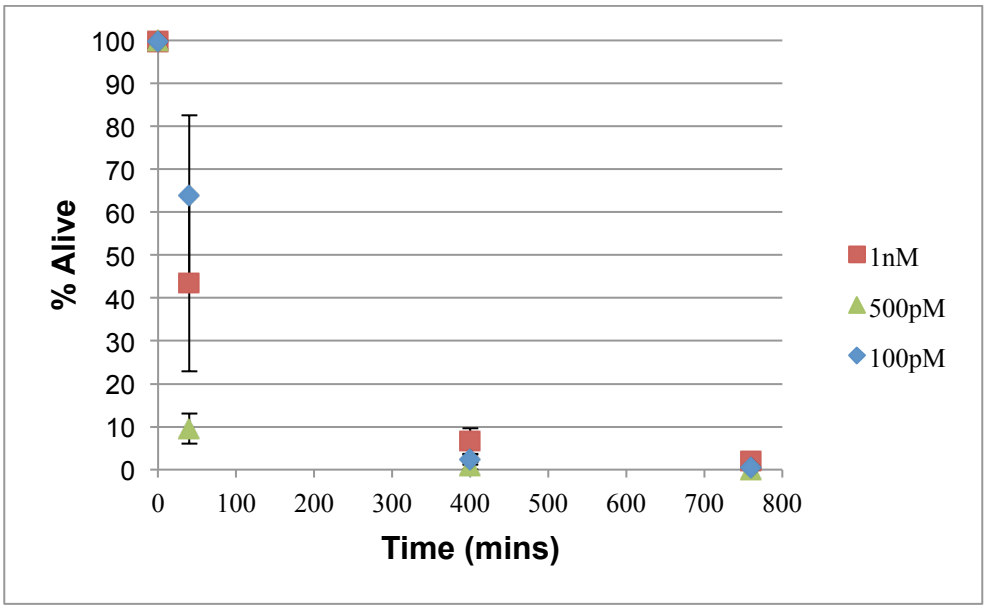

Figure 4.6: Viability of cells incubated with varying concentrations of gold nanoparticles modified with either: TOP: PEG 5K, $(RGD)_4$ only or BOTTOM: PEG 5K, $(RGD)_4$ with and NLS and then illuminated at 514nm for 30 minutes. All experiments were done in triplicates. Error bars denote standard error in the percent of live cells at a given time point.

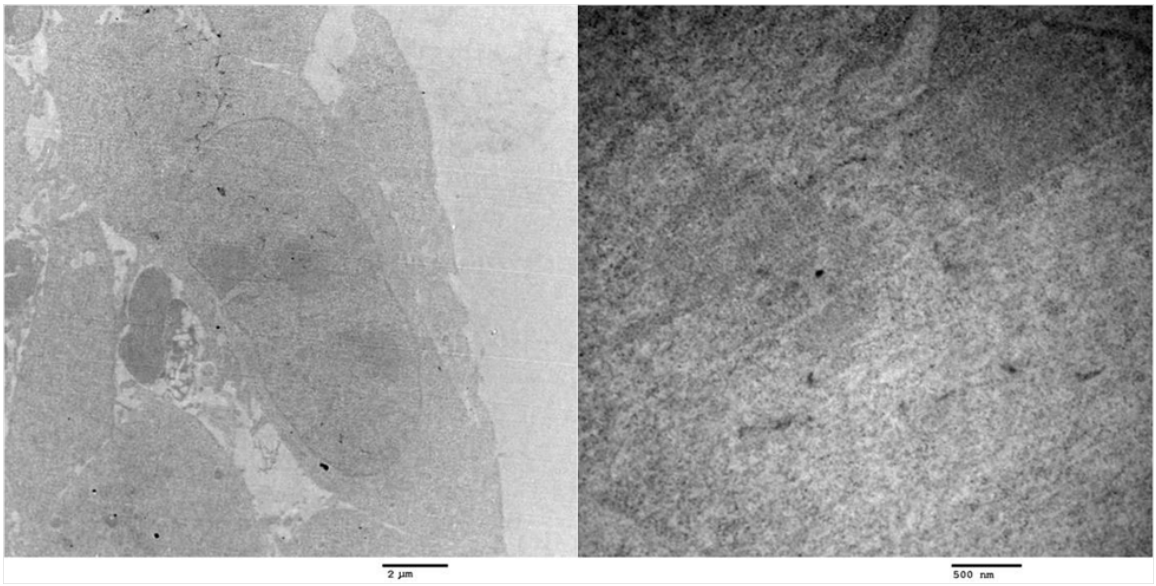

Figure 4.7: TEM confirmation of nuclear delivery in cells that were incubated with 500pM of gold nanoparticles modified with PEG 5K, $(RGD)_4$ and NLS peptides. LEFT: 5700X magnification, RIGHT: 13500 X magnification of the nucleus of the same cell. Appropriate scale bars are below each image.

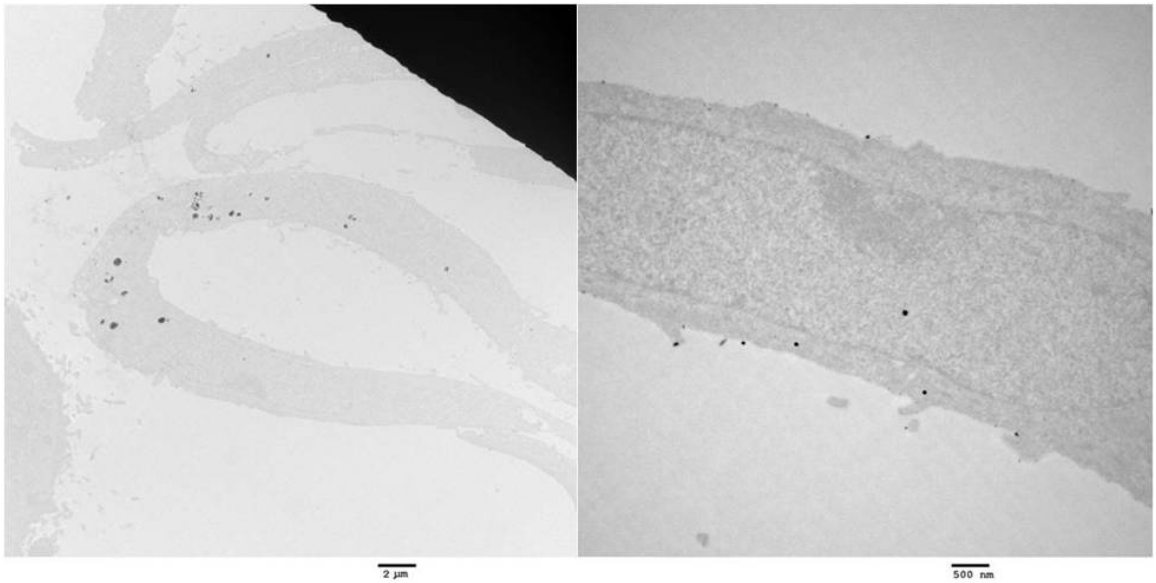

Figure 4.8: TEM confirmation of nuclear delivery in cells that were incubated with 1nM of gold nanoparticles modified with PEG 5K, $(RGD)_4$ and NLS peptides. LEFT: 5700X magnification, RIGHT: 13500 X magnification of the nucleus of the same cell. Appropriate scale bars are below each image.

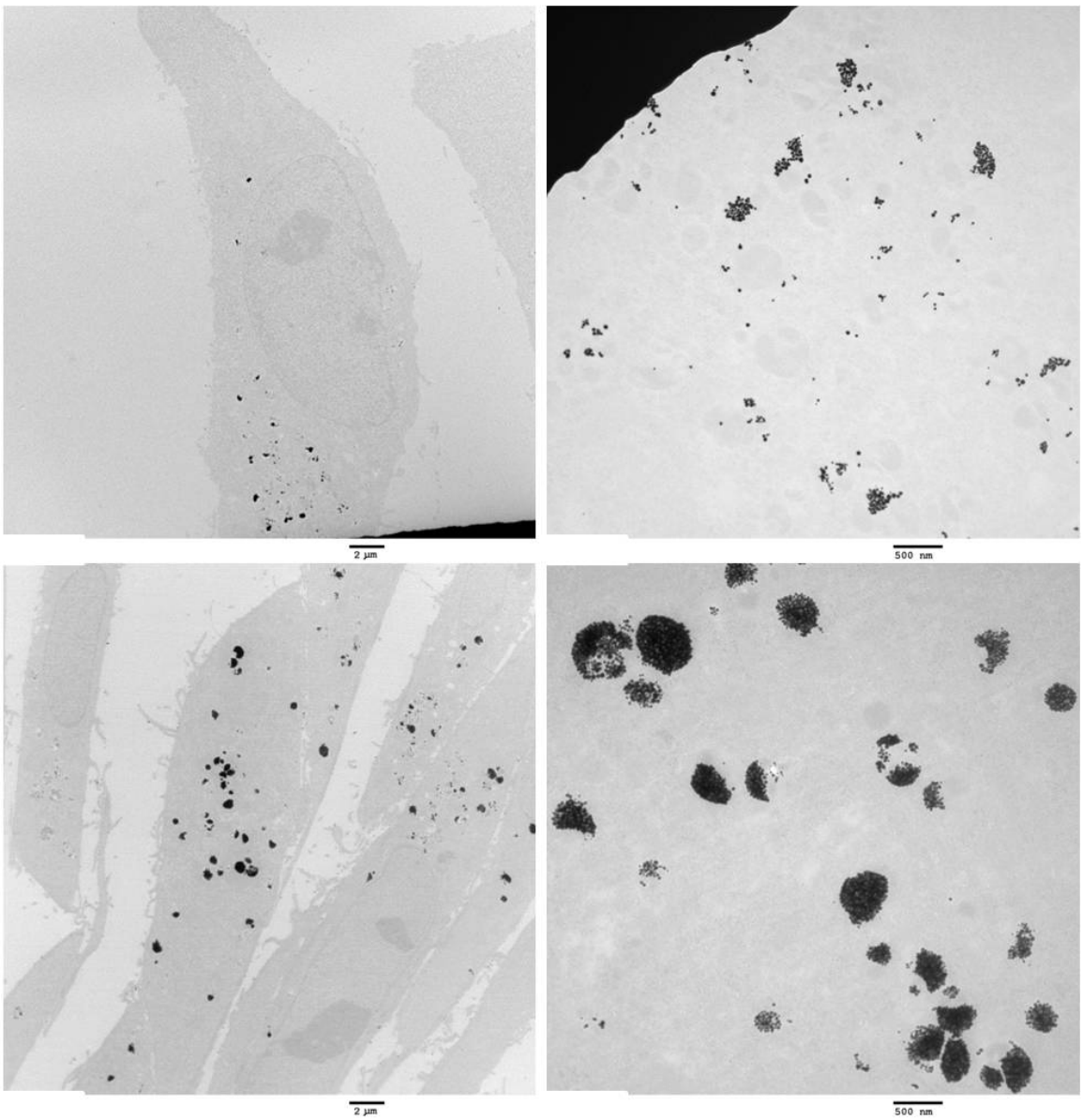

Figure 4.9: Comparison of the fate of gold nanoparticles once they are taken up by the cancer cell for TOP: 500pM and BOTTOM: 1nM nanoparticle concentrations. TEM images on the left are 5700X magnification and TEM images on the right are 13500X magnification of the same cells. Appropriate scale bars are below each image.

4.8 References

1. Boisselier, E.; Astruc, D., Gold nanoparticles in nanomedicine: preparations, imaging, diagnostics, therapies and toxicity. *Chemical Society Reviews* **2009,** *38* (6), 1759-1782.

2. Beija, M.; Li, Y.; Duong, H. T.; Laurent, S.; Vander Elst, L.; Muller, R. N.; Lowe, A. B.; Davis, T. P.; Boyer, C., Polymer-gold nanohybrids with potential use in bimodal MRI/CT: enhancing the relaxometric properties of Gd(III) complexes. *Journal of Materials Chemistry* **2012,** *22* (40), 21382-21386.

3. Xie, M. R.; Ding, L.; You, Z. W.; Gao, D. Y.; Yang, G. D.; Han, H. J., Robust hybrid nanostructures comprising gold and thiol-functionalized polymer nanoparticles: facile preparation, diverse morphologies and unique properties. *Journal of Materials Chemistry* **2012,** *22* (28), 14108-14118.

4. Han, S. Y.; Guo, Q. H.; Xu, M. M.; Yuan, Y. X.; Shen, L. M.; Yao, J. L.; Liu, W.; Gu, R. A., Tunable fabrication on iron oxide/Au/Ag nanostructures for surface enhanced Raman spectroscopy and magnetic enrichment. *Journal of Colloid and Interface Science* **2012,** *378*, 51-57.

5. Guo, X.; Zhang, Q.; Sun, Y. H.; Zhao, Q.; Yang, J., Lateral Etching of Core-Shell Au@Metal Nanorods to Metal-Tipped Au Nanorods with Improved Catalytic Activity. *Acs Nano* **2012,** *6* (2), 1165-1175.

6. Jain, S.; Hirst, D. G.; O'Sullivan, J. M., Gold nanoparticles as novel agents for cancer therapy. *British Journal of Radiology* **2012,** *85* (1010), 101-113.

7. Link, S.; El-Sayed, M. A., Shape and size dependence of radiative, non-radiative and photothermal properties of gold nanocrystals. *International Reviews in Physical Chemistry* **2000,** *19* (3), 409-453.

8. Tkachenko, A. G.; Xie, H.; Liu, Y. L.; Coleman, D.; Ryan, J.; Glomm, W. R.; Shipton, M. K.; Franzen, S.; Feldheim, D. L., Cellular trajectories of peptide-modified gold particle complexes: Comparison of nuclear localization signals and peptide transduction domains. *Bioconjugate Chemistry* **2004,** *15* (3), 482-490.

9. Nativo, P.; Prior, I. A.; Brust, M., Uptake and intracellular fate of surface-modified gold nanoparticles. *Acs Nano* **2008,** *2* (8), 1639-1644.

10. Huang, H. C.; Barua, S.; Sharma, G.; Dey, S. K.; Rege, K., Inorganic nanoparticles for cancer imaging and therapy. *Journal of Controlled Release* **2011,** *155* (3), 344-357.

11. Chial, H. J.; Thompson, H. B.; Splittgerber, A. G., A Spectral Study of the Charge Forms of Coomassie Blue-G. *Analytical Biochemistry* **1993,** *209* (2), 258-266.

12. von Maltzahn, G.; Park, J. H.; Agrawal, A.; Bandaru, N. K.; Das, S. K.; Sailor, M. J.; Bhatia, S. N., Computationally Guided Photothermal Tumor Therapy Using Long-Circulating Gold Nanorod Antennas. *Cancer Research* **2009,** *69* (9), 3892-3900.

13. Choi, J.; Yang, J.; Bang, D.; Park, J.; Suh, J. S.; Huh, Y. M.; Haam, S., Targetable Gold Nanorods for Epithelial Cancer Therapy Guided by Near-IR Absorption Imaging. *Small* **2012,** *8* (5), 746-753.

14. El-Sayed, I. H.; Huang, X. H.; El-Sayed, M. A., Selective laser photo-thermal therapy of epithelial carcinoma using anti-EGFR antibody conjugated gold nanoparticles. *Cancer Letters* **2006,** *239* (1), 129-135.

15. Ray, P. C.; Khan, S. A.; Singh, A. K.; Senapati, D.; Fan, Z., Nanomaterials for targeted detection and photothermal killing of bacteria. *Chemical Society Reviews* **2012,** *41* (8), 3193-3209.

16. Pissuwan, D.; Cortie, C. H.; Valenzuela, S. M.; Cortie, M. B., Functionalised gold nanoparticles for controlling pathogenic bacteria. *Trends in Biotechnology* **2010,** *28* (4), 207-213.

17. Pustovalov, V.; Babenko, V., Computer modeling of optical properties of gold ellipsoidal nanoparticles at laser radiation wavelengths. *Laser Physics Letters* **2005,** *2* (2), 84-88.

18. Takami, A.; Kurita, H.; Koda, S., Laser-induced size reduction of noble metal particles. *Journal of Physical Chemistry B* **1999,** *103* (8), 1226-1232.

19. Letfullin, R. R.; Joenathan, C.; George, T. F.; Zharov, V. P., Laser-induced explosion of gold nanoparticles: potential role for nanophotothermolysis of cancer. *Nanomedicine* **2006,** *1* (4), 473-480.

Chapter 5 Conclusions & Future Directions

5.1 Conclusions

The dissertation research details the fabrication, optimization, and implementation of polymeric and gold nanoparticles for biomedical applications, namely photothermal therapy and nuclear delivery. Taken together, this research contributes to the motivation of further development of nanoparticle-mediated therapies end goal of widespread clinical use.

Chapter 2 is a proof of principle study describing the first ever use of the FDA approved Coomassie blue dye in photothermal therapy. The research presented substantiates the capability of the CB-PAA nanoparticles to serve as a platform for a multimodal therapeutic approach (photoacoustic imaging[1], visual surgical delineation[2] [3] [4] [5], and now PTT). Polymeric nanoparticles have been FDA approved for clinical studies due to their apparent high therapeutic factor and much research has been done on biocompatible, biodegradable, and bio-eliminable hydrogel nanoparticle platforms[6]. Although poly(acrylamide) gel is not FDA approved for use in nanoparticle mediated PTT of cancer cells, it has been successfully utilized in *in vivo* and *in vitro* studies for many years. PAA has also been used successfully in implants in animal models[7]. The pharmacokinetics, biodistribution, bioelimination, and toxicity of PAA gel nanoparticles have been studied *in vivo* and no acute toxicity has been associated with potentially

therapeutic doses [6]. Thus, it is feasible that PAA gel nanoparticles will gain future FDA approval. The covalently-linked Coomassie blue polyacrylamide nanoparticles were shown to be very effective in causing PTT induced thermolysis in HeLa cells for varying nanoparticle concentrations and treatment times. Exploitation of this newly demonstrated PTT function of the nanoparticles could be easily incorporated with the visual delineation, and photoacoustic modalities as a part of a multifunctional approach to cancer detection and treatment using a single nanoparticle administration.

Chapter 3 details the precise surface engineering of gold nanoparticles for nuclear delivery in cancer cells. The gold nanoparticles used in these studies were fabricated using a physical method, femtosecond laser ablation, instead of the conventional chemical method, endowing the nanoparticles with chemically free, *virgin* surfaces[8]. The use of gold nanoparticles with *virgin* surfaces enabled a systematic study on how nanoparticle-cell interactions are dictated by the surface chemistry of the nanoparticles and the ability of optimizing the ratio of functional ligands so as to achieve optimal, cell specific, nuclear delivery. Prior research[9] demonstrated that multiple ligands are needed for effective and efficient nuclear delivery of nanoparticles. The “Sequential Conjugation” method implemented in these studies enabled the stepwise optimization of the surface of the nanoparticle so as to achieve colloidal stability, high intracellular uptake, extended incubation times with no resulting toxicity, and nuclear delivery confirmed using transmission electron microscopy. Furthermore, the highly efficient intracellular delivery and subsequent nuclear delivery was achieved with

a concentration that is *at least* an order of magnitude less than what has been previously reported.

A comparative study of the efficacy of photothermal therapy on cancer cells when treatment is mediated by gold nanoparticle located predominately within the nucleus in contrast to when the gold nanoparticles are predominantly in the cytoplasm is described in **Chapter 4.** This chapter builds on the positive results of the previous chapter on nuclear delivery and the differences in efficacy relative to nanoparticle location, treatment time, and nanoparticle concentration were studied. We hypothesized that PTT mediated by nanoparticles would be more effective overall, and that longer treatment times and higher concentrations would yield the best outcomes in decreased cell viability. Little to no decrease in cell viability was found in control experiments measuring dark toxicity associated with the nanoparticles and decreased viability due to irradiation with no nanoparticles. Overall, the efficacy of PTT mediated by gold nanoparticles with NLS peptide (nearly complete cell death was observed for all concentrations within 6 hours of treatment) was higher than when PTT of cells that were incubated with gold nanoparticles without NLS. Also, the behavior of the cell viability curves depending on whether or not the gold nanoparticles had been modified with NLS peptide and not treatment time. Higher nanoparticle concentrations did not yield higher cell death and intracellular nanoparticle fate studies showed that incubation with the highest gold nanoparticle concentration resulted in the sequestration of large clumps of the nanoparticles within cell compartments.

5.2 Future Directions

5.2.1 Clinical Use of CB-PAA Nanoparticles

The delineation and photoacoustic studies involving the targeted CB-PAA nanoparticles described in **Chapter 1** were previously employed *in vivo* and *ex vivo,* respectively for treatment of brain tumors, at NPs doses of up to 250 mg/kg of rat mass. The most effective nanoparticle concentrations used in the PTT experiments ranged from 0.6-1.2 mg/mL. Based on these two studies, scaling this dosage up for clinical administration to a healthy human yields a dosage on the order of 10^4 mg. Such a dose may lead to unwanted side effects and compromise patient health. Some alternatives to circumvent this problem include utilizing a more intense light source, local injection of the nanoparticles, and improved targeting. The LED array used in the PTT studies has a maximum intensity on the order of mW, which combined with the varying concentrations led to nearly complete cell death for concentrations higher than 0.4 mg/mL. If the lower concentrations were coupled with a more intense light source (FDA approved level of 30 mJ/cm^2) and concomittantly lower treatment times, clinical relevant dosages of the nanoparticles could then be used for effective PTT after delineation, excision, and photoacoustic imaging of the tumors. It is important that the more intense light source not cause damage to healthy cells with no NPs. If a pulsed laser is utilized, the critical time threshold for treatment requires that the pulse be shorter then the time it takes for the heat to dissipate away from the target. This time threshold is approximately 1ms, which would allow the use

of a light source several orders of magnitude stronger than the light source utilized in these experiments. Other forms of cancer can likely be treated using targeted CB-PAA NPs, however, in the absence of surgical excision of the primary tumor, only superficial cancers would be treatable (e. g. melanomas), as the maximum absorbance of the NPs does not allow for penetration depths exceeding tens of millimeters of healthy tissue.

Further, local injection after excision would also contribute to clinical performance of these nanoparticles. Staining of the cancer cells occurred within a few hours of administration in the *in vivo* studies. Thus local injection would help to ensure that CB-PAA uptake in the region of interest is high enough for subsequent PTT. Also, as noted previously, for optimal future use in clinical studies, the nontoxic CB-PAA nanoparticles would need to be further optimized to be targeted, as previously demonstrated, and engineered to be biodegradable so as to decrease the probability of nanoparticle uptake into healthy cells and ensure that all nanoparticles are eventually bioeliminated from the patient post-treatment. F3 peptide was utilized previously, but a more efficient targeting moiety also be used to decrease the probability of uptake by noncancerous cells. It should be noted that even with all of the aforementioned optimizations and improvements, clinical applications of treatment to tumors may be limited if multiple dosing of the nanoparticles is not feasible. An initial dose of the NPs will result in the accumulation of the NPs on the exterior of the tumor (i.e. delineation of the tumor's margins), leaving the majority of the tumor devoid of any therapeutic agents. After irradiation treatment and subsequent cell death, the

newly exposed tumor cells would be free to proliferate. Additional administrations of the CB-PAA NPs, ideally through local intravenous injection, would be necessary to ensure a high probability of the destruction of the entire tumor.

5.2.2 Faster Nuclear Delivery of Surfaced Modified Gold Nanoparticles

Our recent studies have successfully achieved nuclear delivery of partially PEGylated Au NPs conjugated with both $(RGD)_4$ and NLS peptides to the cell nucleus. The intracellular delivery of the Au NPs is mediated by endocytosis; the NPs are trapped in an endosome-lysosome complex and taken inside of the cell. To achieve nuclear delivery Au NPs must escape out of the endosome-lysosome complex into cytoplasm so that they can freely bind to importin α/β and be transported into nucleus. Nuclear delivery of the biocompatible, multitargeted Au NPs was successful; however, the process takes 40-50 hours, which may limit future development of nuclear-based novel technologies in diagnosis and therapeutics. A large decrease in the time necessary for delivering gold nanoparticles into cell nucleus is the most important next step. A peptide that will deliver the Au NPs into cells' cytosol without involving endocytosis is required. Toward this aim, F3 peptide could be utilized as the cell targeting molecule and NLS peptide for nuclear targeting. F3 peptide is a 31-amino acid fragment of human high mobility group protein 2 (HMGN2), which targets cancer cells through the nucleolin receptor. F3 peptide has been utilized in previous studies

conducted in the Kopelman lab, for achieving cellular internalization of NPs via a pathway that avoids endocytosis[10 11].

5.2.3 Strategies for Improving Gold Nanoparticle-Mediated Photothermal Therapy

As discussed in Chapter 1, the fraction of C_{abs}/m or Q_{abs}/r determine the heating and therefore the cell kill. One way to increase C_{abs}/m or Q_{abs}/r and therefore therapeutic heating is through the use gold nanoparticle clusters. Gold nanoparticle clusters have many advantages in reference to therapeutic uses including:

- A shift in the maximum absorption wavelength toward the NIR range and "therapeutic window"
- Less worry of scattering/interaction with biological tissues
- Enhanced photoacoustic signal.

Aggregation of the gold nanoparticles utilized in the studies outlined in **Chapters 3 & 4** would increase the scenarios in which this form of PTT could be exploited. If the nanoparticles could be administered in the colloidal form and then induced to form aggregates within the cell, a new form of photothermal therapy could be realized. One way to achieve such aggregation is through the use of peptides that target severely overexpressed receptors on the cancer cell membrane. This would increase the probability of the nanoparticles being taken up as aggregates. A two-step process in which the cells are irradiated initially at 520nm and subsequently at the maximum wavelength of the nanoparticle clusters, may

result in an increase in the efficiency of cell killing. Both intracellular uptake and nuclear delivery are heavily influenced by the size of the nanoparticle, so aggregate should not be too large. With the use of a microabsorber, the maximum absorbance of the nanoparticle aggregates within the cell can be measured and the photothermal experiments outlined in **Chapter 4** can be repeated using the two-step irradiation. The differences in overall dosage required for cell kill, the therapeutic efficiency with respect to concentration and illumination times, and the cell death pathways would be of great interest.

5.3 References

1. Ray, A.; Wang, X. D.; Lee, Y. E. K.; Hah, H. J.; Kim, G.; Chen, T.; Orringer, D. A.; Sagher, O.; Liu, X. J.; Kopelman, R., Targeted blue nanoparticles as photoacoustic contrast agent for brain tumor delineation. *Nano Research* **2011,** *4* (11), 1163-1173.

2. Orringer, D. A.; Chen, T.; Huang, D. L.; Armstead, W. M.; Hoff, B. A.; Koo, Y. E. L.; Keep, R. F.; Philbert, M. A.; Kopelman, R.; Sagher, O., The Brain Tumor Window Model: A Combined Cranial Window and Implanted Glioma Model for Evaluating Intraoperative Contrast Agents. *Neurosurgery* **2010,** *66* (4), 736-743.

3. Orringer, D. A.; Koo, Y. E. L.; Chen, T.; Kim, G.; Hah, H. J.; Xu, H.; Wang, S. Y.; Keep, R.; Philbert, M. A.; Kopelman, R.; Sagher, O., In vitro Characterization of a targeted, dye-loaded nanodevice for intraoperative tumore delineation. *Neurosurgery* **2009,** *64* (5), 965-971.

4. Orringer, D. A.; Koo, Y. E.; Chen, T.; Kopelman, R.; Sagher, O.; Philbert, M. A., Small Solutions for Big Problems: The Application of Nanoparticles to Brain Tumor Diagnosis and Therapy. *Clinical Pharmacology & Therapeutics* **2009,** *85* (5), 531-534.

5. Nie, G. C.; Hah, H. J.; Kim, G.; Lee, Y. E. K.; Qin, M.; Ratani, T. S.; Fotiadis, P.; Miller, A.; Kochi, A.; Gao, D.; Chen, T.; Orringer, D. A.; Sagher, O.; Philbert, M. A.; Kopelman, R., Hydrogel Nanoparticles with Covalently Linked Coomassie Blue for Brain Tumor Delineation Visible to the Surgeon. *Small* **2012,** *8* (6), 884-891.

6. Koo, Y. E. L.; Reddy, G. R.; Bhojani, M.; Schneider, R.; Philbert, M. A.; Rehemtulla, A.; Ross, B. D.; Kopelman, R., Brain cancer diagnosis and therapy with nanoplatforms. *Advanced Drug Delivery Reviews* **2006,** *58* (14), 1556-1577.

7. Davis, B. K., Diffusion in polymer gel implants. *Proceedings of the National Academy of Sciences of the United States of America* **1974,** *71* (8), 3120-3123.

8. Qian, W.; Murakami, M.; Ichikawa, Y.; Che, Y., Highly Efficient and Controllable PEGylation of Gold Nanoparticles Prepared by Femtosecond Laser Ablation in Water. *Journal of Physical Chemistry C* **2011,** *115* (47), 23293-23298.

9. Tkachenko, A. G.; Xie, H.; Coleman, D.; Glomm, W.; Ryan, J.; Anderson, M. F.; Franzen, S.; Feldheim, D. L., Multifunctional gold nanoparticle-peptide complexes for nuclear targeting. *Journal of the American Chemical Society* **2003,** *125* (16), 4700-4701.

10. Reddy, G. R.; Bhojani, M. S.; McConville, P.; Moody, J.; Moffat, B. A.; Hall, D. E.; Kim, G.; Koo, Y. E. L.; Woolliscroft, M. J.; Sugai, J. V.; Johnson, T. D.; Philbert, M. A.; Kopelman, R.; Rehemtulla, A.; Ross, B. D., Vascular targeted nanoparticles for imaging and treatment of brain tumors. *Clinical Cancer Research* **2006,** *12* (22), 6677-6686.

11. Wang, S. Y.; Fan, W. Z.; Kim, G.; Hah, H. J.; Lee, Y. E. K.; Kopelman, R.; Ethirajan, M.; Gupta, A.; Goswami, L. N.; Pera, P.; Morgan, J.; Pandey, R. K., Novel Methods to Incorporate Photosensitizers Into Nanocarriers for Cancer Treatment by Photodynamic Therapy. *Lasers in Surgery and Medicine* **2011,** *43* (7), 686-695.